RADAR-DETECTED MESOCYCLONE TILT IN TORNADIC AND NONTORNADIC SUPERCELLS

A Thesis

by

MICHELLE MARIE SERINO

Submitted to the Office of Graduate and Professional Studies of
Texas A&M University
in partial fulfillment of the requirements for the degree of

MASTER OF SCIENCE

Chair of Committee,	Christopher Nowotarski
Committee Members,	Craig Epifanio
	Matthias Katzfuss
Head of Department,	Ping Yang

Spring 2018

Major Subject: Atmospheric Sciences

ABSTRACT

While supercell thunderstorms are the storms with the greatest potential of producing tornadoes, the majority of supercells do not produce tornadoes. Recent work has demonstrated that low-level (LL) vertical wind shear and lifting condensation level (LCL) height in the storm inflow region are the most promising discriminators between tornadic and nontornadic supercells. It is anticipated that as the horizontal distance between the LL and mid-level (ML) mesocyclones (mesocyclone tilt) decreases, the likelihood and intensity of a tornado increase. It is expected that there is an orientation of both LL vertical shear and lower LCL height that results in a smaller mesocyclone tilt. This study builds a climatology of radar data to distinguish between tornadic and nontornadic supercells. Level-II and -III Weather Surveillance Radar-1988 Doppler data were collected and processed for a subset of isolated supercells in the contiguous United States from 2009 to 2015.

From this initial climatology, LL and ML azimuthal wind shear maxima are located, representing the LL and ML mesocyclones, and the horizontal distance between each maximum is calculated during the evolution of each supercell. Results connecting the mesocyclone tilt to aspects of the near-storm environment, including LL shear magnitude and orientation and LCL height, will be discussed. Characteristics of the storm environment are obtained from proximity soundings derived from the Rapid Update Cycle and Rapid Refresh model analyses. Statistical and observational analyses of the climatology and of individual case studies will be presented.

Significantly tornadic supercells are associated with low LCL heights, strong southwesterly LL vertical wind shear, and critical angles below 100°. While smaller mesocyclone tilts are often associated with significant tornadoes, there is considerable overlap between distributions, suggesting that nontornadic and weakly tornadic storms may also have small tilts. There may be also a balance of shear orientation that moderates the position of outflow to result in a small positive or negative mesocyclone tilt. Further consideration should be given to the LL kinematic storm environment when discriminating between tornadic and nontornadic supercells.

This work is for my family and friends, especially my parents, boyfriend, and graduate student cohort, who all supported me during my research. I also dedicate this to my junior and senior high school teachers, university professors, and other scientists who cultivated my passion for science and discovery.

CONTRIBUTORS AND FUNDING SOURCES

This work was supported by a thesis committee consisting of Dr. Christopher Nowotarski (advisor) and Dr. Craig Epifanio of the Department of Atmospheric Sciences, and Dr. Matthias Katzfuss of the Department of Statistics.

The National Oceanic and Atmospheric Administration (NOAA) Storm Events Database is maintained at https://www.ncdc.noaa.gov/stormevents. The Level-II radar data were provided by the National Centers for Environmental Information (NCEI), NOAA, U.S. Department of Commerce. The Level-III Mesocyclone Detection Algorithm data were obtained from the NOAA Severe Weather Data Inventory. The RUC-2 and RAP Analyses were provided by the NOAA Earth Systems Research Laboratory - Global Systems Division and Earth Modeling Branch and accessed through the NOAA National Operational Model Archive and Distribution System. The Global Land One-km Base Elevation Project (GLOBE) data were provided with the following reference: The GLOBE Task Team and others (Hastings, David A., Paula K. Dunbar, Gerald M. Elphingstone, Mark Bootz, Hiroshi Murakami, Hiroshi Maruyama, Hiroshi Masaharu, Peter Holland, John Payne, Nevin A. Bryant, Thomas L. Logan, J.-P. Muller, Gunter Schreier, and John S. MacDonald), eds., 1999. The Global Land One-kilometer Base Elevation Digital Elevation Model, Version 1.0. National Oceanic and Atmospheric Administration, National Geophysical Data Center, 325 Broadway, Boulder, Colorado 80305-3328, U.S.A. Digital database on the World Wide Web (http://www.ngdc.noaa.gov/mgg/topo/globe.html) and CD-ROMs. The Weather and

Climate Toolkit is maintained by the NCEI, NOAA, U.S. Department of Commerce. The National Center for Atmospheric Research (NCAR) Command Language (NCL) was provided with the following reference: The NCAR Command Language (Version 6.3.0) [Software]. (2015). Boulder, Colorado: NCAR/CISL/VETS. doi:10.5065/D6WD3XH5. The NCL forum, Stack Overflow website, Guido Cioni, Felicia Guarriello, Matthew Mahalik, Christopher Nowotarski, Kiel Ortega, Dennis Shea, and Kevin Smalley provided code assistance. All other work conducted for this thesis was completed by the student independently.

This work was funded by National Science Foundation grant AGS-1446342.

TABLE OF CONTENTS

1. INTRODUCTION AND LITERATURE REVIEW

1.1 Introduction

The National Oceanic and Atmospheric Administration (NOAA) reports the average warning time for a tornado as 13 minutes, although not every thunderstorm that produces a tornado receives a timely warning (Brotzge and Erickson 2009). Significant (≥EF2 on the Enhanced Fujita Scale) tornadoes cause the majority of damage, injuries, and deaths in the United States, and most of these tornadoes are created by supercell thunderstorms (Markowski and Richardson 2009). However, most supercells are not tornadic, so it is vital for forecasters to differentiate between tornadic and nontornadic storms (Trapp et al. 2005). While the forecasting and warning of supercells have been refined, additional research is required to improve discrimination between tornadic and nontornadic supercells. Until operational forecast models are capable of accurately predicting and resolving tornadoes, operational improvements must continue to be made from atmospheric observations. In order to better understand how aspects of the near-storm environment affect supercell structure as it relates to tornadogenesis, this work investigates mesocyclones observed by the weather radar network across the United States combined with proximity-sounding information representative of the near-storm environment from model analyses.

1.2 Background

Supercell thunderstorms (Figure A-1) have been studied in increasing detail over the past several decades (e.g., Byers and Braham 1948; Whiting and Bailey 1957; Browning 1965; Lemon and Doswell 1979; Rotunno and Klemp 1985; Doswell and Burgess 1993; Markowski and Richardson 2009; Davies-Jones and Markowski 2013). The defining characteristic of a supercell thunderstorm is a deep, persistent, cyclonically rotating updraft: a mesocyclone. The mesocyclone is about 2-10 km wide, extends through the middle of the troposphere, and has vertical vorticity on the order of 10^{-2} s^{-1}. Much is understood about the formation and dynamics of mesocyclones aloft, but those of mesocyclones near the ground are less established, especially as related to tornadogenesis (Markowski and Richardson 2009). Though they are not the most common type of thunderstorm, supercells are more likely to produce the strongest tornadoes in comparison to other types of thunderstorms (Markowski and Richardson 2009). These tornadoes, although not as common as the weaker EF0-EF1 categories, disproportionately cause the majority of damage and injuries in the United States (Markowski and Richardson 2009).

1.2.1 Supercell Tornadoes

There are three general phases leading to supercellular tornadogenesis: midlevel (ML; 3-6 km) mesocyclone formation, low-level (LL; 0-2 km) mesocyclone formation, and intensification of LL vertical vorticity to tornado strength. Questions still remain regarding the last phase (Markowski and Richardson 2009). Initially, a supercell forms

as a positively buoyant convective updraft tilts ambient horizontal vorticity associated with strong vertical wind shear into the vertical, which creates two counter-rotating vortices on either side of the updraft. This is defined by the tilting term of the vertical vorticity equation (the third term of Equation 1):

$$\frac{\partial \zeta}{\partial t} = -\mathbf{v} \cdot \boldsymbol{\nabla}\zeta + \zeta\frac{\partial w}{\partial z} + \boldsymbol{\omega_H} \cdot \boldsymbol{\nabla_H} w \qquad (1)$$

where $\boldsymbol{\omega_H}$ is the horizontal environmental vorticity, and $\boldsymbol{\nabla_H} w$ is the horizontal gradient of the vertical velocity. If the initial horizontal vorticity is streamwise, the cyclonic vortex is advected towards and co-located with the updraft as tilting occurs, via the first term of Equation 1, where **v** is the three-dimensional environmental velocity, and $\boldsymbol{\nabla}\zeta$ is the gradient of vertical vorticity (the advection term; Davies-Jones 1984). Streamwise vorticity is the component of the horizontal vorticity that is parallel to the storm-relative wind, and it can be enhanced by baroclinic generation in the LL horizontal buoyancy gradient at the edge of the forward-flank outflow (Davies-Jones 1984). This tilting and advection creates an area of cyclonically rotating, upward-moving air at midlevels in the atmosphere (generally >1 km above ground level [AGL]) and establishes the first stage in supercell formation. If preexisting vertical vorticity is absent near the ground (<500 m), this process that generates the ML mesocyclone is not sufficient to generate the near-ground rotation. This is because, if horizontal vorticity is tilted only by an updraft, the resulting vertical vorticity moves upward away from the ground as it is created (Davies-Jones and Brooks 1993). Therefore, during the intermediate phase, a downdraft is required to tilt LL horizontal vorticity vertically at the surface or to advect vertical vorticity from aloft, in order to generate cyclonic rotation at the ground (Markowski and

Richardson 2008; Davies-Jones and Markowski 2013). The baroclinicity within the rain-cooled, negatively buoyant downdraft and outflow air is also suggested to be essential to the development of horizontal rotation near the ground, such that the near-ground circulation that precedes tornadogenesis develops in the supercell outflow or cold pool (e.g., Brandes 1984; Davies-Jones and Brooks 1993; Markowski et al. 2008; Dahl 2015). These preceding phases set the stage for supercell tornadogenesis. The vertical vorticity now present at the surface must be stretched in order to achieve tornado strength through conservation of angular momentum (the second term of Equation 1). This is the stretching term, where $\partial w / \partial z$ is the change in vertical velocity with height. This stretching may be achieved by the upward nonlinear dynamic vertical perturbation pressure gradient force (VPPGF). The VPPGF is enhanced when a vertical gradient in vorticity exists between the LL mesocyclone and the ML mesocyclone, which creates an area of dynamically forced updraft and LL convergence of negatively buoyant cold pool air beneath the ML mesocyclone (Markowski and Richardson 2009). Thus, the stretching of the column of vertical vorticity into a tornado is dependent upon the strength of the ML mesocyclone, the amount of circulation in the outflow, the negative buoyancy of the outflow, and the position of the ML mesocyclone relative to the portion of the outflow containing appreciable circulation (Markowski and Richardson 2009).

Byers and Braham (1948) and Lemon and Doswell (1979) established that some separation between low- and midlevels is favored in steady thunderstorms because that positioning prevents precipitation and downdrafts from contaminating updrafts. While too much or too strong of outflow beneath the ML mesocyclone is likely detrimental to

near-ground rotation or supercell longevity, because near-ground circulation generally forms in negatively buoyant supercell outflow, dynamic lifting is required to intensify near-ground rotation to tornado strength. Thus, it is expected that horizontal alignment between the ML and LL mesocyclone is a requisite condition for tornadogenesis. A recent numerical modeling study by Guarriello et al. (2018) determined that as the distance between the LL and ML mesocyclones decreases, the strength of the surface vertical vorticity increases. This complements the deductions made from observational studies.

1.2.2 Environmental Factors Influencing Supercellular Tornadogenesis

Though many environmental parameters influence the likelihood of tornadoes, Figure A-2 illustrates that lifting condensation level (LCL) height and LL vertical wind shear are both particularly effective in discriminating between tornadic and nontornadic supercell environments (e.g., Rasmussen and Blanchard 1998; Markowski et al. 2002; Thompson et al. 2003; Craven and Brooks 2002; Markowski and Richardson 2009; Markowski and Richardson 2014). Tornadic supercell environments are associated with relatively low LCL heights, an indicator of high boundary layer relative humidity, which have generally been found to result in warmer, less negatively buoyant cold pools (Markowski and Richardson 2009; Markowski and Richardson 2014). Cold pools with smaller equivalent potential temperature deficits have been shown to be associated with lower LCL heights, decreased evaporation of precipitation, and decreased cooling of outflow air (Markowski et al. 2002). However, it remains unclear if increased

precipitable water content associated with lower LCL heights could ultimately lead to more negatively buoyant outflow due to greater precipitation production (Lerach and Cotton 2012). The competing effects of colder, denser, more negatively buoyant outflow on tornadogenesis have been described as a "Goldilocks problem" (Markowski and Richardson 2009). Colder outflow, relative to the environment, is associated with more baroclinicity and a greater likelihood of creating vertical vorticity at the ground. Conversely, more negatively buoyant outflow is less responsive to dynamically driven vertical acceleration, which reduces stretching of near-ground vorticity. The detrimental effects of overly cold outflow on tornadogenesis have been shown by both observations of supercell outflow (Markowski et al. 2002; Grzych et al. 2007) and numerical simulations (Brooks et al. 1994; Gilmore and Wicker 1998; Markowski and Richardson 2014). The influence of LCL height on the position of the LL circulation relative to the ML mesocyclone is expected to be crucial to the effectiveness of the LL dynamic forcing described above. Lower LCL height results in less evaporative cooling of supercell outflow, which creates a moderate, relatively less dense, cold pool that may move forward more slowly and be less likely to surge out ahead of the overlying mesocyclone (Figure A-3):

$$c = k\sqrt{gH\frac{\rho_2-\rho_1}{\rho_1}} \quad (2)$$

where c is the forward speed of the cold pool, k is a correction factor, g is gravity, H is the depth of the cold pool, ρ_2 is the density of the cold pool and ρ_1 is the density of the environment (Markowski and Richardson 2010). This could allow the ML mesocyclone, and the entire supercell, to persist and have opportunity to intensify.

Climatological studies using both modeled and observed supercell proximity soundings have associated tornadic environments with increased LL vertical wind shear (e.g., Rasmussen and Blanchard 1998; Markowski et al. 2003; Thompson et al. 2003; Craven and Brooks 2002). More recently, studies suggest that both the magnitude and direction of the vertical wind shear vector tend to be relevant to tornadogenesis. Observations of a hodograph with winds veering (turning clockwise with height) at low levels have suggested that strong, streamwise environmental horizontal vorticity near the ground is more favorable for tornado formation (Esterheld and Giuliano 2008; Kis and Straka 2010; Nowotarski and Jensen 2013). Regardless of similar storm-relative helicity and deep-layer shear, hodographs with strong streamwise vorticity and southerly shear near the ground are more likely to produce tornadic storms than those with mostly crosswise vorticity and easterly shear (Esterheld and Giuliano 2008). The influence of LL shear on supercells may have two components. One, concluded by Wicker (1996), is that the orientation of the horizontal vorticity of the surface inflow may be augmented by baroclinic generation of horizontal vorticity. The second component is that increased near-ground streamwise vorticity may contribute to a stronger mesocyclone aloft and enhance the LL upward-directed dynamic VPPGF. This may intensify the convergence of vertical vorticity near the ground (Markowski and Richardson 2009, Markowski and Richardson 2014).

The influence of both the orientation and magnitude of LL vertical wind shear on the position of the LL circulation relative to the ML mesocyclone are also believed to be crucial to the strength of the LL dynamic forcing described above. There is expected to

be an optimal orientation of LL vertical wind shear relative to the supercell gust front that may inhibit the forward motion of the outflow, preventing the cold pool from surging ahead of itself and undercutting the LL mesocyclone from the inflow. Guarriello et al. (2018) determined that there was a favored orientation of LL vertical wind shear (Figure A-4) that contributed to a decreased distance between the LL and ML mesocyclones. In their simulations, these simulations had the strongest near-ground vertical vorticity. It is also thought that strong LL storm-relative (SR) winds opposing the gust front are likely to decrease the forward speed of the cold pool, such that outflow does not undercut the overlying mesocyclone.

1.2.3 Radar Observations of Mesocyclones

The Next Generation Weather Radar (NEXRAD) network of WSR-88Ds is an effective and efficient platform with which to observe the properties of numerous supercells across the contiguous United States (CONUS), a subset of which will form the climatology presented in this study. The NEXRAD network utilizes advanced Doppler radar capabilities, real-time signal processing techniques, meteorological algorithms, and automated processing to generate numerous, continuously-updated analysis products (Klazura and Imy 1993). The radars can resolve a mesocyclone of typical size and are continuously scanning throughout the day with prescribed scan patterns for storm conditions. They do possess limitations, which will be discussed below.

Previous studies (e.g., Browning 1965; Burgess et al. 1976; Lemon et al. 1977; Zrnić et al. 1985; Burgess and Lemon 1990) have used the United States radar network to evaluate supercell evolution. The storm mode is initially determined from a visual evaluation of radar reflectivity, and supercell thunderstorms often share a similar echo shape, vertical reflectivity profile, three-dimensional, and velocity signatures (Burgess and Lemon 1990; Thompson et al. 2012). Burgess and Lemon (1990) confirmed that most supercells are fairly large, elliptical thunderstorms with large values of reflectivity and a hook echo (indicative of a mesocyclone). These storms display a weak echo region and a midlevel echo overhang, both indicative of an updraft, on the right rear flank (Burgess and Lemon 1990). The mesocyclone of a supercell can be seen in Doppler velocity as two adjacent radial velocity peaks of opposite sign and is identified operationally with the National Severe Storms Laboratory (NSSL) mesocyclone detection algorithm (MDA; Burgess and Lemon 1990; Desrochers and Donaldson 1992; Lee and White 1998; Stumpf et al. 1998). After scanning circulations in four dimensions, a mesocyclone is identified when a strong, symmetrical circulation exists over at least two elevation angles (Klazura and Imy 1993; Stumpf et al. 1998). Those circulations are subsequently refined to meet additional strength and duration criteria (Stumpf et al. 1998). The above characteristics tend to be most pronounced when a mesocyclone, and thus, a supercell, is strongest. These features do not, however, have the same predictive ability for tornadoes. While a tornado is more likely to form from a strong supercell that possesses these properties, that formation is not guaranteed (Burgess and Lemon 1990). Although it has shortcomings that will be described below,

the NEXRAD network is an extensive one that can be used efficiently to study many mesocyclones across large spatial and temporal extents.

1.3 Hypothesis

Based on what is already established and the gaps that remain, this work consists of two relatively unexplored hypotheses to test with a climatology of radar observations of supercell mesocyclones. The first is that tornadic supercells have a smaller distance between the LL and ML mesocyclones, which will be referred to hereafter as the mesocyclone tilt. As described above, it is expected that supercell tornadoes require a strong dynamic VPPGF co-located with antecedent vertical vorticity near the ground, and that this is only possible when the mesocyclone tilt is small. This relationship is expected to lead to stronger LL convergence of buoyant air and stretching of LL vertical vorticity that is necessary to form a tornado (Markowski and Richardson 2009).

The second hypothesis is that the mesocyclone tilt is influenced by some combination of the environmental LCL height and the LL vertical wind shear magnitude and orientation. Regarding the thermodynamics, it is expected that lower LCL height allows a more humid environment, less evaporative cooling of supercell outflow, a moderate cold pool, and less negatively buoyant outflow. This may result in a slower forward speed of the cold pool, which may be less likely to move ahead underneath the LL mesocyclone and suppress LL vorticity stretching and tornado formation. Regarding the dynamics, it is expected that a favored orientation and magnitude of LL vertical wind shear or storm relative winds opposing the supercell gust front will slow the forward speed of the cold

pool. This slower outflow may also be less likely to undercut the LL mesocyclone and suppress LL vorticity stretching.

The findings from Guarriello et al. (2018) further encourage this investigation, which aims to verify the modeling results with observations. The hypotheses will be evaluated by comparing mesocyclone tilt, LCL height, and LL shear in both tornadic and nontornadic supercells. Section 2 will describe the data and methods used in this study and the results. Section 3 will discuss present results, while Section 4 will discuss conclusions and limitations of this study.

2. METHODS

To evaluate the hypotheses described above, this study builds a climatology of isolated supercells, as defined by Thompson et al. (2002), Grams et al. (2012), and Smith et al. (2012), using a subset of cases from 2009 through 2015 compiled by Smith et al. (2014). Most severe weather reports associated with supercells are qualitatively described in the National Center for Environmental Information Storm Event Database. The cases were limited to the CONUS because some environmental data (Weygandt 2017, Figure A-5), which will be described in Section 2.2 and adequate radar coverage, are only available over this domain (Maddox et al. 2002; Benjamin et al. 2016). Processing, which will be described in Section 2.1.3, includes quality controlling radar reflectivity and velocity data and calculating the LL & ML layers of azimuthal shear. The LL and ML maximum azimuthal shear values and locations were identified, which acted as proxies for the strength and center of each mesocyclone (Zrnić et al. 1985). For each supercell at each radar volume time, mesocyclone tilt was calculated, and the variation of this tilt was examined throughout the lifetime of each supercell. To investigate the environmental component of the hypothesis, model grid-point proximity soundings from supercell inflow regions were used to find the LCL height and the LL vertical wind shear magnitude and orientation, and these parameters were also compared throughout the lifetime of each supercell.

2.1 Radar Data

The radar data used were Level-II reflectivity and mean radial velocity and the Level-III MDA (Desrochers and Donaldson 1992; Lee and White 1998; Stumpf et al. 1998; Ansari et al. 2010). Data from 56 tornadic and 32 nontornadic supercells were included only throughout the duration of the MDA-detected mesocyclone associated with each storm, or multiple mesocyclones if they occurred. Furthermore, only MDAs persisting for two consecutive volume scans (approximately 10 minutes) were considered. The MDA for each supercell must have been relatively consistent, and if there was no MDA identified for at least thirty minutes, the case was discarded. If there were multiple MDAs at any one time, the one closest to the lowest-level azimuthal shear maximum was used to define the position of the storm. The "midpoint" of each storm, which was utilized during data analysis, was defined as the beginning of a tornado for tornadic supercells and as the middle of the MDA lifespan for nontornadic supercells. NOAA's Weather and Climate Toolkit (WCT) was used to inspect each supercell case to determine the duration and consistency of each MDA and to differentiate between multiple concurrent MDAs. This software also ensured that selected MDAs were within 100 km of a radar, which allowed both the LL and ML mesocyclones to be fully sampled and avoided excessive beam spreading with distance.

The WSR-88D network (Radar Operations Center 2017, Figure A-6) is the most practical platform with which to study numerous supercells across a large area and over a large span of time. In precipitation modes, the radars sample a full volume roughly every 4.5 minutes (Torres and Curtis 2006). They provide a base reflectivity product to

a range of 460 km with an azimuthal resolution of 0.5° and a range gate resolution of 250 m (Torres and Curtis 2007). Doppler velocity and spectrum width products are both provided to a range of 300 km with an azimuthal resolution of 0.5° and a range gate resolution of 250 m (Torres and Curtis 2007). Dual-polarization (dual-pol) capability was implemented starting in 2011, and these resolutions apply to both the single- and dual-pol radar products. The radar in Evansville, Indiana, remains in Legacy Resolution (reflectivity: 1.0° x 1.0 km; Doppler velocity and spectrum width: 1.0° x 1.0 km; Torres and Curtis 2007). Several radars located on military bases operate with Legacy Resolution, as well. Because tornadoes can be smaller than 250 meters in diameter, and because both tornadoes and supercells can evolve on time scales shorter than 4.5 minutes, the WSR-88D network may miss important structural details as they rapidly evolve through space and time. However, the supercell mesocyclone is nearly always detectable on radar, and the spatial resolution is adequate for the purposes of this study. In the western United States, the spatial coverage is degraded because of mountainous terrain that blocks the radar signal (Klazura and Imy 1993). However, supercells in these unmeasured areas are infrequent, and their exclusion from this study was not expected to significantly affect the results (Agee et al. 2016; Guo et al. 2016). An ideal option would be a platform such as mobile Doppler radar with higher spatial and temporal resolutions. While their resolutions are much finer, those radars can only practically cover a small area at a time and have not sampled enough supercells for an adequate climatology.

A few other limitations of the NEXRAD network affect the choices in methodology for this study. One is the linear spreading of the radar beam with distance from the radar. This may result in a feature that only partially fills the transmitted beam volume and thus the inaccurate resolution of that storm, despite adequate resolution closer to the radar (Wood and Brown 1997; Wood and Brown 2000). In addition to beam spreading, the beam elevation increases with distance from the radar due to the positive elevation angle and the curvature of the earth. At ranges farther than about 100 km, the beam starts to overshoot the LL portion of a supercell. For both beam spreading and elevation issues, supercells are not considered outside of a range of 100 km from any radar in this study. A related problem regarding the radar beam is that mesocyclone azimuthal shear magnitude and location measurements can be dependent on the mesocyclone location within the beam sampling volume, regardless of range (Wood and Brown 2000). For this study, these inaccuracies may result in under- or over-estimated mesocyclone strength and range (Wood and Brown 2000; Wood et al. 2001). Another potential problem is attenuation of the radar beam by hydrometeors and aerosols, which is common in strong thunderstorms and at long ranges (Rinehart 2010). However, the WSR-88D radar operates with a 10-cm wavelength, in the microwave S-band, which minimizes these effects compared to shorter wavelength radars (Rinehart 2010). Two related problems that can be difficult to correct are range folding and velocity aliasing. Range folding results in an echo appearing closer to the radar than it actually is, and velocity aliasing results in the underestimation of large velocity values (Rinehart 2010). Range folding can be mitigated with an automatic pulse repetition frequency (Ice

et al. 2013; Chrisman 2013), and the data processing discussed later remedies both range folding and velocity aliasing (Lakshmanan et al. 2007a; Lakshmanan et al. 2010; Miller et al. 2013; Lakshmanan et al. 2014). Steiner and Smith (2002) detailed the problem of anomalous propagation when specific atmospheric temperature, humidity, and pressure conditions cause the radar beam to refract toward or away from the ground more than is standard. If this occurs, the beam may over or underestimate target heights (Steiner and Smith 2002; Lakshmanan et al. 2007a; Lakshmanan et al. 2010); however, quality control algorithms mitigate this problem somewhat. A last and minor problem is that radar returns may be contaminated with ground clutter and biological echoes, but both of these artifacts are largely removed by the data processing (Lakshmanan et al. 2007a; Lakshmanan et al. 2010).

2.2 Near-storm Environment Data

Hourly analyses from the 20- and 13-km Rapid Update Cycle Version 2 (RUC-2) and the 13-km Rapid Refresh (RAP) were used to improve processing of the radar data and to calculate characteristics of the near-storm environment. Vertical profiles from analysis data were used because observed soundings are not available with sufficient temporal or spatial resolution to describe the near-storm environment of each supercell, and it has been shown that these data are an acceptable proxy for observed soundings (Thompson et al. 2003; Benjamin et al. 2016). To dealias the radar radial velocity data, wind profiles obtained from the model analysis at the hour most closely corresponding to the midpoint in the lifespan of each storm were used. For assessing the near-storm

environmental characteristics, data one hour before the midpoint of each supercell lifespan and 60 km away from the supercell in the storm inflow region were used following recommendations of Potvin et al. (2010). These time and distance constraints were found to yield the most accurate representation of environmental inflow ingested into a supercell (Potvin et al. 2010). If contamination from nearby storms was present, these constraints were expanded to 40-80 km away from the supercell and/or at the storm midpoint (Potvin et al. 2010). Until the influence of nearby storms on the inflow of other storms is more clearly understood, this study is limited to isolated supercells and analysis-derived soundings to those that appeared to be most representative of the unaltered inflow environment (Thompson et al. 2003; Nowotarski and Markowski 2016). The RUC-2/RAP data report pressure, altitude, temperature, dew point, relative humidity, wind speed and direction, LCL height, and convective available potential energy (CAPE). The wind speed, wind direction, and storm motion were used to calculate the environmental LL vertical wind shear and the storm-relative wind speed and direction.

While the RUC-2 Analysis has been determined to be representative of supercell environments, the model does have shortcomings. Predominantly, any temperature errors are within about 0.5 °C, mixing ratio errors are within about 0.2 g kg^{-1}, and wind speeds tend to be about 1 m s^{-1} too strong from the surface to 400 hPa (Thompson et al. 2003; Turner et al. 2003). Overall, the analyses tended to be a little too cool and dry at the surface, but these errors are comparable to those of radiosonde measurements available during the time the RUC-2 was still in use (Thompson et al. 2003; Turner et al.

2003). Because of negative biases in surface temperatures and mixing ratios, surface-based CAPE was generally underestimated by 300–500 J kg^{-1} (Thompson et al. 2003). Both 0-1 km and 0-6 km shear vector magnitudes contain about a 2 m s^{-1} error (Thompson et al. 2003). Despite these shortcomings, when the RUC-2 Analysis was used, it provided sufficient storm environment information for this study.

2.3 Processing Radar Data

The radar data were processed with the Warning Decision Support System-Integrated Information (WDSS-II) algorithms, developed at the National Severe Storms Laboratory (NSSL; Lakshmanan et al. 2007b). Unlike other platforms, WDSS-II allows data interpretation and visualization from multiple radars and multiple radar platforms, creating a more complete network of data when necessary (Lakshmanan et al. 2007b).

Table A-1 illustrates the chronology of the WDSS-II algorithms, mentioned hereafter in italics, used to process the radar data for each case. *w2qcnn* (*w2qcnndp* for dual-pol data) uses a neural network to remove non-precipitating radar reflectivity due to anomalous propagation, biological echoes, and ground clutter (Lakshmanan et al. 2007a; Lakshmanan et al. 2010; Lakshmanan et al. 2014). However, *w2qcnn* edits data every vertical column, making it is impossible to preserve quality data aloft if the lower levels are contaminated (Lakshmanan et al. 2007a). Because the algorithm ingests surface temperature at the radar site, its performance is degraded in the transitional months of spring and fall, which are included in this study (Lakshmanan et al. 2010). *w2qcnndp* improves upon these methods, which was used with dual-polarization radar data during

and after 2012 (Lakshmanan et al. 2014). *w2qcnn* identifies biological echoes if reflectivity values are equal to or below 35 dBZ, which may cause weaker precipitation echoes embedded among biological echoes to be identified as all biological or as all precipitation (Lakshmanan et al. 2010). *dealias2d* corrects velocity aliasing using environmental soundings from the RUC-2/RAP analyses (Lakshmanan 2012). *topoBreak* uses Global Land One-kilometer Base Elevation (GLOBE) gridded, quality-controlled, Digital Elevation Model (DEM) data to convert data to altitude AGL. This information is used by *w2circ*, which calculates layers of azimuthal shear AGL using a linear least squares derivatives (LLSD) method (Smith and Elmore 2004; Lakshmanan et al. 2013; Miller et al. 2013; Newman et al. 2013). The algorithm calculates the LL azimuthal shear field between 0-2 km AGL and the ML azimuthal shear field between 3-6 km AGL from the radial velocity (Figure A-7):

$$\frac{\partial V_r}{\partial s} = \frac{\sum s_{ij} V_{ij} w_{ij}}{\sum s_{ij}^2 w_{ij}} \quad (3)$$

where V_r is the radial velocity, s is the coordinate in the azimuthal direction, s_{ij} is the arc length from the center point of the calculation to the point (i,j), V_{ij} is the radial velocity at (i,j), and w_{ij} is a positive weight function that differs according to the current point (i,j) (Newman et al. 2013). These definitions allow a necessary delineation between the LL and ML altitudes for assessing mesocyclone tilt and ensures that shear at higher altitudes does not mask shear at lower altitudes. Ideally, LL would be defined at the ground, but that is not possible with the WSR-88D, as even the lowest elevation angle is 0.5° above the surface. This algorithm accounts for degradation of azimuthal shear resolution with range from the radar and corrects for errors caused by random variations

in radar beam position (Smith and Elmore 2004; Lakshmanan et al. 2013; Miller et al. 2013; Newman et al. 2013). However, *w2circ* can create azimuthal shear in areas of low reflectivity, this may exacerbate the biological bias and result in either an under- or overestimation of shear for weak, nontornadic mesocyclones, and mask the true locations of the LL and ML mesocyclones (Smith and Elmore 2004; Lakshmanan et al. 2013; Miller et al. 2013). Because azimuthal shear is a derived product, it is susceptible to noise that may not have been completely removed from the velocity field (Lakshmanan et al. 2013). *w2merger* converts the calculated shear fields and quality controlled data to a two-dimensional, latitude-longitude grid (Lakshmanan et al. 2006; Lakshmanan and Humphrey 2013). All of these algorithms are compatible with both NEXRAD and non-NEXRAD radar data.

After the radar data were processed, the tilt between the LL and ML maximum azimuthal shear was calculated as the distance between the coordinates of the LL and ML mesocyclones using the Vincenty formula, which treats the earth as an oblate spheroid. When comparing the locations of the LL and ML mesocyclones, they must occur temporally close together to ensure an accurate comparison. Because the radar, after scanning the LLs, takes some time to move up to the MLs to scan, a correction (University Corporation for Atmospheric Research 2018, Figure A-8) was applied to account for that time lapse. This was done by utilizing the storm motion and shifting the coordinates of the ML mesocyclone backwards to where it would have been at the time the radar scanned the LL portion of the storm. The storm motion was calculated based on the distance the storm moved during an elapsed time. The definition of each

mesocyclone tilt is dependent on the direction of supercell motion, such that the tilt is designated as positive (negative) if the ML mesocyclone is ahead of (behind) the LL mesocyclone relative to the storm motion.

3. RESULTS

3.1 Supercell Case Studies

Several case studies will demonstrate the data and methods used in the larger climatology that encompasses the majority of this work. These cases include both tornadic and nontornadic supercells with relatively large and small mesocyclone tilts and will highlight points relevant to the relationships of LL vertical wind shear, LCL height, and mesocyclone tilt.

3.1.1 05 June 2009 – Tornadic Supercell, Small Mesocyclone Tilt

An EF2 tornado associated with a supercell in southeastern Wyoming occurred in the afternoon of 05 June 2009 (Figure A-9). In general, the mesocyclone tilt was small in the time leading up to and during the tornado (Figure A-9b), which is consistent with the first hypothesis motivating this study. This suggests that, throughout the majority of the storm, the ML mesocyclone remained relatively close to the LL mesocyclone, which is a hypothesized requirement for the LL mesocyclone to strengthen and produce a tornado. It was only immediately before the dissipation of the tornado that the mesocyclone tilt abruptly increased.

A moderately low LCL height of 930 m AGL was present in the storm environment for this supercell (Figure A-9c). While cold pool and outflow characteristics cannot generally be assessed via radar observations alone, this would suggest limited sub-cloud evaporation of hydrometeors, perhaps resulting in a relatively

weak cold pool. Consequently, a positive mesocyclone tilt might be expected (all else being equal), based on slower propagation of weaker outflow. LL vertical wind shear (Figure A-9d) was only moderate, as well, with values of 1.20 m s^{-1} from 188° (0-500 m AGL) and 5.73 m s^{-1} from 248° (0-1 km AGL). The surface SR wind was 13.03 m s^{-1} from 125°, which would oppose the southeastward motion of the supercell and its outflow and also favor a positive mesocyclone tilt. Esterheld and Giuliano (2008) define the critical angle as the angle between the 0-500 m vertical wind shear and the surface SR wind vectors. Based on the modeling study (Guarriello et al. 2018), tornadic supercells tend to have critical angles near 90°, indicating enhanced streamwise vorticity at the surface (Esterheld and Giuliano 2008). This tornadic supercell had an unexpected critical angle of about 68°. While the LCL and LL wind shear characteristics suggest that a positive tilt would be expected, that orientation was not observed until late in the tornado's life. Thus, LCL and LL wind shear may not be the best predictors of mesocyclone alignment in this case.

3.1.2 18 April 2013 – Tornadic Supercell, Large Mesocyclone Tilt

An EF1 tornado associated with a supercell in southwestern Oklahoma occurred during the evening of 18 April 2013 (Figure A-10). In general, the mesocyclone tilt was large and sporadic in the time leading up to and during the tornado, which is unexpected with a tornadic supercell. While this may suggest that, throughout the majority of the storm, the ML mesocyclone remained relatively displaced from the LL mesocyclone, Figure A-10a suggests that there were two prominent maxima in azimuthal shear. Thus,

despite alternation in the maximum LL and ML shear locations, the tornadic shear maximum may have always been in close proximity to an overlying mesocyclone. Moreover, the mesocyclone tilt is relatively small immediately before the tornado (Figure A-10b).

A moderately high LCL height of 1155 m AGL was present in the storm environment for this supercell, suggesting enhanced evaporation beneath the clouds and perhaps resulting in a relatively strong cold pool (Figure A-10c). This type of outflow moves more quickly and is expected to result in a negative mesocyclone tilt (all else being equal). LL vertical wind shear was moderate (Figure A-10d), with values of 3.81 m s^{-1} from 198° (0-500 m AGL) and 6.25 m s^{-1} from 232° (0-1 km AGL). The surface SR wind was 16.86 m s^{-1} from 122°, which would minimally affect the northeastward motion of the supercell and would oppose the southeastward motion of the outflow and favor a positive mesocyclone tilt. This tornadic supercell had a critical angle of about 105°, which was more expected based on the findings of Esterheld and Giuliano (2008). Based on the hypotheses of this study, the LCL and LL wind shear characteristics suggested both a negative and positive tilt during this supercell, and both of those orientations were observed, with a negative tilt occurring more often. It is possible that the LCL height was the determining factor regarding the mesocyclone tilt for this particular supercell.

3.1.3 24 December 2009 – Nontornadic Supercell, Small Mesocyclone Tilt

A nontornadic supercell in southwestern Arkansas occurred during the night of 24 December 2009 (Figure A-11). In general, the mesocyclone tilt was small throughout the storm, which, by itself would seem to be conducive for tornadogenesis (Figure A-11b). This suggests that, throughout the majority of the storm, the ML mesocyclone remained relatively close to the LL mesocyclone. Despite this favorable orientation, the weak instability of 216 J kg^{-1} of CAPE may have inhibited tornadogenesis.

A low LCL height of 98 m AGL was present in the storm environment for this supercell, which is consistent with the moist low levels on the sounding in Figure A-11c. This suggests curbed evaporation of hydrometeors and a weak cold pool. This type of outflow would move more slowly and is expected to result in a positive mesocyclone tilt (all else being equal). LL vertical wind shear was fairly strong (Figure A-11d), with values of 7.61 m s^{-1} from 198° (0-500 m AGL) and 11.86 m s^{-1} from 222° (0-1 km AGL). The surface SR wind was 15.95 m s^{-1} from 69°, which would oppose the northeastward motion of the supercell outflow and also favor a positive mesocyclone tilt. This storm had a critical angle of about 50°, which is consistent with other nontornadic supercells (Esterheld and Giuliano 2008). Both the LCL and LL wind shear characteristics suggested a positive tilt occurring during this supercell, which was observed.

3.1.4 22 May 2014 – Nontornadic Supercell, Large Mesocyclone Tilt

A nontornadic supercell in eastern Maryland occurred in the afternoon of 22 May 2014 (Figure A-12). In general, despite multiple areas of relatively strong azimuthal shear both aloft and at low-levels (Figure A-12a), the mesocyclone tilt was large during this storm (Figure A-12b), which may have contributed to its nontornadic nature. This suggests that, throughout the majority of the storm, the ML mesocyclone remained relatively displaced from the LL mesocyclone. Even with a moderately unstable environment, with 1940 J kg^{-1} of CAPE, the supercell did not strengthen to produce a tornado.

A moderately high LCL height of 1197 m AGL was present in the storm environment for this supercell, suggesting enhanced sub-cloud evaporation and perhaps resulting in a relatively strong cold pool (Figure A-12c). This type of outflow moves more quickly and is expected to result in a negative mesocyclone tilt (all else being equal). LL vertical wind shear was moderate (Figure A-12d), with values of 1.19 m s^{-1} from 270° (0-500 m AGL) and 3.27 m s^{-1} from 300° (0-1 km AGL). The surface SR wind was 12.14 m s^{-1} from 102°, which would oppose the southeastward motion of the supercell outflow and favor a positive mesocyclone tilt, which was observed only once during the storm. Similar to the tornadic, large-tilt case study, this supercell had a critical angle of about 12°, which was expected. The LCL and LL wind shear characteristics both suggested a negative tilt during this supercell, and that orientation was observed during the majority of the storm.

3.2 Supercell Climatology

The climatology consists of 88 tornadic and nontornadic supercells across the CONUS from 2009-2015, spanning all seasons and times of day (Figure A-13). The collection of storms was used to test the hypotheses considered in this study. This was done qualitatively with box-and-whisker plots and quantitatively with linear correlation.

3.2.1 Hypothesis 1 – Mesocyclone Tilt

The first hypothesis is that tornadic supercells are expected to have a small mesocyclone tilt. It is thought that a smaller tilt will enhance the stretching of vertical vorticity at the surface and form a tornado. While the median tilt magnitude is similar for nontornadic, weakly tornadic, and significantly tornadic supercells in this climatology, a smaller range of tilts tends to be present with significant supercells (Figure A-14a). The same pattern is observed for mesocyclone tilts during all tornadic and nontornadic activity of every supercell (Figure A-14b). Similarly, the median tilt tends to decrease just before weak tornadoes (Figure A-15b), and the tilt spread tends to decrease just before the beginning of significant tornadoes (Figure A-15c). Near tornado initiation, the parent mesocyclones tend to have smaller tilts, which may support enhanced stretching of LL vertical vorticity, when compared to other instances during the supercell. Though these findings are supportive of the notion that tornadic supercells are associated with smaller mesocyclone tilts, there is considerable overlap in the distributions, which suggests this relationship may not be as strong as anticipated.

3.2.2 Hypothesis 2 – LCL Height and LL Vertical Wind Shear

LL vertical wind shear and LCL height have been shown to be promising discriminators between tornadic and nontornadic supercells. Figure A-16 reproduces the plot from Craven Brooks (2002; herein Figure A-2), showing the relationship between the types of supercells in this climatology and their storm environments. The tornadic supercells tend to form in environments with lower LCL heights and larger values of LL shear, though some weakly tornadic supercells defy this paradigm. The second, multi-part hypothesis is that lower LCL heights and aspects of the LL wind profile are associated with smaller mesocyclone tilts.

It is thought that a lower LCL height results in a more humid environment, which may prevent the supercell outflow from moving quickly and creating a large mesocyclone tilt. Significantly tornadic supercells tend to occur in environments within a narrow range of low LCL heights, whereas nontornadic and weakly tornadic supercells tend to occur within a wider range of higher heights, suggesting that humid environments favor significant tornadoes in this climatology (Figure A-17a), consistent with earlier work. Despite this, there appears to be no significant correlation between LCL height and mesocyclone tilt (Figure A-17b), which suggests that LCL height has little bearing on mesocyclone tilt in this climatology.

The second part of this hypothesis is that there is a preferred magnitude and orientation of LL vertical wind shear that favors significantly tornadic supercells through promotion of smaller mesocyclone tilts. As expected, significant and nontornadic supercells in this climatology have the largest and smallest medians of 0-1 km shear

magnitude, respectively (Figure A-18a). There is a positive correlation between mesocyclone tilt and 0-1 km shear magnitude (Figure A-18d), suggesting that as the shear increases, this suppresses the motion of the supercell outflow and favors a positive tilt. However, this correlation is only statistically significant (to the 5% significance level) for the total sample and significantly tornadic supercells. This correlation, perhaps counterintuitively, suggests that if shear is too strong, it could suppress the outflow motion so severely as to create a large positive tilt that would be detrimental to vorticity stretching and tornadoes. Most of the supercells in this study tend to occur in environments with a westerly component of the 0-1 km shear and a median direction from the southwest, with the significantly tornadic storms occurring across a smaller range of directions (Figures A-18b and A-18c). For significantly tornadic supercells, there is a negative relationship between mesocyclone tilt and shear direction (Figure A-18e), suggesting that as the LL shear becomes more westerly, the outflow encounters less resistance and is able to move ahead, resulting in a negative tilt. However, this is contrary to previous work (e.g., Markowski and Richardson 2010). This tendency appears to be present due to the outer limits of the distribution, and upon visually removing them, the relationship weakens. At this level, none of the supercells occurred with easterly shear, making comparison with the findings of Guarriello et al. (2018; herein Figure A-4) difficult.

It is possible that shear over even shallower layers than 1 km reveals important differences related to mesocyclone tilt. In a layer closer to the surface, nontornadic supercells have the smallest median of 0-500 m vertical wind shear magnitude, and

significantly tornadic supercells appear over a larger range of shear magnitudes (Figure A-19a). For significantly tornadic supercells, there is a moderate positive correlation between mesocyclone tilt and 0-500 m shear (Figure A-19d), suggesting that as the shear increases, this suppresses the motion of the supercell outflow and favors a positive tilt. Similar to the 0-1 km shear layer, it is possible that excessively strong 0-500 m shear may suppress outflow so severely and create a large tilt that would suppress supercell strengthening. All of the supercells tend to occur in environments with southwesterly 0-500 m shear, with the significant storms occurring across a smaller range of shear directions (Figure A-19b). For significantly tornadic supercells, there is a moderate negative correlation between mesocyclone tilt and shear direction, as seen in the 0-1 km shear layer (Figure A-19e). This suggests that as the LL shear becomes more westerly, the outflow encounters less resistance and is able to move ahead, resulting in a negative tilt. However, this is contrary to previous work (e.g., Markowski and Richardson 2010), as with the 0-1 km shear layer. This tendency appears to be present due to the outer limits of the distribution, and upon visually removing them, the relationship weakens. In this layer, only one supercell was associated with northerly shear, and only two with the easterly shear (Figure A-19c) that showed favorable in Guarriello et al. (2018; herein Figure A-4).

Because the surface SR wind may also control the positioning and motion of supercell outflow, in addition to LL shear orientation, it is valuable to explore its influence, as well. It is believed that strong SR wind oriented against the forward motion of the outflow may hinder it and result in a positive mesocyclone tilt. While the

climatology does not suggest a correlation between surface SR wind magnitude and mesocyclone tilt, most of the supercells occur with SR winds below 20 m s^{-1} (Figure A-20b). All of the supercells have about the same median, with the nontornadic occurring over a wider range of values (Figure A-20a). For significant supercells, the SR wind tends toward the east, as most of those strong storms have an easterly component to their vector motion (Figure A-20c). It may be that the easterly SR wind inhibits the forward motion of the outflow and favors a more positive mesocyclone tilt, resulting in a stronger supercell. Figure A-20d shows a moderately negative trend in tilt for significantly tornadic supercells as the SR wind veers from easterly to southerly, suggesting that the outflow encounters less resistance and is able to move ahead of the ML mesocyclone.

Recent work has suggested the importance of the angle between the 0-500 m vertical wind shear and the surface SR wind vectors (Esterheld and Giuliano 2002; Coffer and Parker 2017). This critical angle may indicate the amount of streamwise horizontal vorticity available at the surface and tends toward 90° in tornadic supercells (Esterheld and Giuliano 2002; Coffer and Parker 2017). In this study, significantly tornadic supercells have a median critical angle around 70°, nontornadic supercells have a median angle around 60°, and weakly tornadic supercells have a median angle closer to the favored 90° (Figure A-21a). Despite those inclinations, however, the significantly tornadic supercells exist over a smaller range than the other storm types. Although there is no significant correlation between the critical angle and mesocyclone tilt, most significantly tornadic supercells have critical angles below 100° (Figure A-21b),

implying that there may be a favored orientation of LL shear and SR wind, which may be more evident in a larger climatology.

4. CONCLUSIONS AND FUTURE WORK

Because the climatology in this study is relatively small, the conclusions are contingent on further study. Significantly tornadic supercells are associated with low LCL heights, strong southwesterly LL vertical wind shear, and critical angles below 100°. Smaller mesocyclone tilts are often associated with significant tornadoes and tornadic times of supercells, but there is considerable overlap between distributions, suggesting that nontornadic and weakly tornadic storms may also have small mesocyclone tilts. Some of these findings contrast with other work. Guarriello et al. (2018) found that easterly LL vertical wind shear results in a more upright mesocyclone, larger near-ground vertical vorticity, and larger near-ground circulation. Although their work found that westerly shear results in large positive mesocyclone tilts, there may be a balance of shear orientation that moderates the position of outflow to result in a small positive or negative mesocyclone tilt. While Esterheld and Giuliano (2008) found that critical angles closer to 90° tend to accompany tornadic supercells, especially significantly tornadic supercells, those conclusions were based on a small sample size. Regardless, further consideration should be given to the LL kinematic storm environment when discriminating between tornadic and nontornadic supercells. Forecasters may give special attention to environments that exhibit traditional supercellular characteristics and that also simultaneously possess low LCL heights, southwesterly LL vertical wind shear, and critical angles below 100°.

These conclusions may be affected by some limitations of the study and by errors inherent in the data and processing methods. The cases contained herein were limited to the WSR-88D NEXRAD network for completeness and practicality, but those radars may neglect some evolutionary mesocyclone features that are smaller than 250 meters and that develop more often than about every 5 minutes (Kumjian et al. 2010). While the network encompasses most of the CONUS, there are some gaps in data coverage between radars, especially west of the Rocky Mountains, and directly above radars in the cone of silence, both of which decrease the sample of measurable supercells.

The algorithms used to process the radar data possess several limitations, detailed in section 2.3, that may have affected the results. Errors in *w2qcnn*, especially before its improvement for use with dual-polarization radar, may have masked upper level radar data and inaccurately differentiated weak precipitation echoes from biological echoes (Lakshmanan et al. 2007a, Lakshmanan et al. 2010). *w2circ* can generate azimuthal shear in areas of low reflectivity, which may exacerbate the biases of *w2qcnn* and result in under- or overestimation of shear for weak, nontornadic mesocyclones, mask the true locations of those LL and ML mesocyclones, and under- or overestimate the resultant mesocyclone tilt magnitudes and orientations (Smith and Elmore 2004; Lakshmanan et al. 2013; Miller et al. 2013). Errors in the calculated mesocyclone tilt may also be present due to mesocyclone cycling (Foote and Frank 1983; French et al. 2008). Because *gribToNetcdf* only reads Analysis data in Gridded Binary (GRIB) 1 format, which was no longer available after March 2012, over half of the cases contained in this work were not quality controlled with a supplementary environmental sounding. There

was also a case before 2012 that did not have GRIB 1 data associated with it, and attempts to convert the data to a readable format were unsuccessful.

While the RUC-2 Analysis has been determined to be representative of supercell environments, the model has weaknesses, detailed in section 2.2, that may have also slightly affected the results. The 0-1 km shear vector magnitude is biased, positively or negatively, by about 2 m s^{-1} (Thompson et al. 2003). Since the greater interest for this study was on the shear vector orientation, this small bias can be overlooked. The analyses tended to be a little too cool and dry at the surface, underestimating surface-based CAPE (Thompson et al. 2003). However, that environmental characteristic was not emphasized for this study.

The statistics performed on the climatology make some assumptions that imperfectly apply to the data. The test for linear correlation between variables assumes a normally distributed, homoscedastic, linear dataset with no outliers. The hypothesis test for significance assumes a large, randomly sampled, homoscedastic, normally distributed dataset. Because this is an observational study, based on the method of case selection, the data distribution cannot be verified as truly normal or randomly sampled. By visually inspecting the correlation plots, it is obvious that some variables are not normally distributed about the regression lines (homoscedastic) and that some outliers are present. All of these shortcomings would be improved with a larger dataset.

For further study, high resolution Doppler on Wheels (DOW) data may be analyzed. Building a larger climatology would increase the robustness of any

conclusions, and considering non-isolated supercells in more complex environments may allow researchers to make more specific conclusions regarding a given supercell.

REFERENCES

Agee, E., J. Larson, S. Childs, and A. Marmo, 2016: Spatial Redistribution of U.S. Tornado Activity between 1954 and 2013. *J. Appl. Meteor. Climatol.*, **55**, 1681–1697.

Ansari, S., M. Phillips, and S. A. Del Greco, 2010: The severe weather data inventory: a geospatial database of severe weather data at NOAA's National Climatic Data Center (NCDC). Pre-prints, *2nd Conf. on International Cooperation in the Earth System Sciences and Services*, Atlanta, GA, Amer. Meteor. Soc., J15.3. [Available online at https://ams.confex.com/ams/pdfpapers/159679.pdf.]

Benjamin, S., S. Weygandt, J. Brown, M. Hu, C. Alexander, T. Smirnova, J. Olson, E. James, D. Dowell, G. Grell, H. Lin, S. Peckham, T. Smith, W. Moninger, J. Kenyon, and G. Manikin, 2016: A North American Hourly Assimilation and Model Forecast Cycle: The Rapid Refresh. *Mon. Wea. Rev.*, **144**, 1669–1694.

Brandes, E., 1984: Vertical Vorticity Generation and Mesocyclone Sustenance in Tornadic Thunderstorms: The Observational Evidence. *Mon. Wea. Rev.*, **112**, 2253–2269.

Brooks, H., C. Doswell, and J. Cooper, 1994: On the Environments of Tornadic and Nontornadic Mesocyclones. *Wea. Forecasting*, **9**, 606–618.

Brotzge, J., and S. Erickson, 2009: NWS Tornado Warnings with Zero or Negative Lead Times. *Wea. Forecasting*, **24**, 140–154.

Browning, K., 1965: The Evolution of Tornadic Storms. *J. Atmos. Sci.*, **22**, 664–668.

Burgess, D., L. D. Hennington, R. J. Doviak, and P. S. Ray, 1976: Multimoment Doppler Display for Severe Storm Identification. *J. Appl. Meteor.*, **15**, 1302–1306.

Burgess, D., and L. R. Lemon, 1990: Severe Thunderstorm Detection by Radar, *Radar in Meteorology*. D. Atlas, Amer. Meteor. Soc., Boston, MA, pp. 619-647. ISBN 978-1-935704-15-7.

Byers, H., and R. Braham, 1948: Thunderstorm Structure and Circulation. *J. Meteor.*, **5**, 71–86.

Chrisman, J., 2013: *Uncovering the Storm*. Radar Operations Center NEXRAD Now, 22, 9-11.

Coffer, B., and M. D. Parker, 2017: Simulated Supercells in Nontornadic and Tornadic VORTEX2 Environments. *Mon. Wea. Rev.*, **145**, 149–180.

Craven, J. P., and H. E. Brooks, 2002: Baseline Climatology of Sounding Derived Parameters Associated with Deep Moist Convection. Preprints, *21st Conf. on Severe Local Storms*, San Antonio, TX, Amer. Meteor. Soc., 16.3. [Available online at https://ams.confex.com/ams/SLS_WAF_NWP/techprogram/paper_46783.htm.]

Dahl, J., 2015: Near-Ground Rotation in Simulated Supercells: On the Robustness of the Baroclinic Mechanism. *Mon. Wea. Rev.*, **143**, 4929–4942.

Davies-Jones, R., 1984: Streamwise Vorticity: The Origin of Updraft Rotation in Supercell Storms. *J. Atmos. Sci.*, **41**, 2991–3006.

Davies-Jones, R., and H. Brooks, 1993: Mesocyclogenesis from a Theoretical Perspective*, The Tornado: Its Structure, Dynamics, Prediction, and Hazards.* C. Church, D. Burgess, C. Doswell, and R. Davies-Jones, *Geophys. Monogr.*, Amer. Geophys. Union, Washington, D. C., pp. 105-114. ISBN 9781118664148.

Doswell, C., and D. Burgess, 1993: Tornadoes and tornadic storms: a review of conceptual models*, The Tornado: Its Structure, Dynamics, Prediction, and Hazards*. C. Church, D. Burgess, C. Doswell, and R. Davies-Jones, *Geophys. Monogr.*, Amer. Geophys. Union, Washington, D. C., pp. 161–172. ISBN 9781118664148.

Davies-Jones, R., and P. Markowski, 2013: Lifting of Ambient Air by Density Currents in Sheared Environments. *J. Atmos. Sci.*, **70**, 1204–1215.

Desrochers, P., and R. Donaldson, 1992: Automatic Tornado Prediction with an Improved Mesocyclone-Detection Algorithm. *Wea. Forecasting*, **7**, 373–388.

Esterheld, J., and Giuliano, D. 2008: Discriminating between Tornadic and Non-Tornadic Supercells: A New Hodograph Technique. *EJSSM*, **3**, 2.

Foote, G., and H. W. Frank, 1983: Case Study of a Hailstorm in Colorado. Part III: Airflow from Triple-Doppler Measurements. *J. Atmos. Sci.*, **40**, 686–707.

French, M., H. B. Bluestein, D. C. Dowell, L. J. Wicker, M. R. Kramar, and A. L. Pazmany, 2008: High-Resolution, Mobile Doppler Radar Observations of Cyclic Mesocyclogenesis in a Supercell. *Mon. Wea. Rev.,* **136**, 4997–5016.

Gilmore, M., and L. Wicker, 1998: The Influence of Midtropospheric Dryness on Supercell Morphology and Evolution. *Mon. Wea. Rev.*, **126**, 943–958.

Grams, J., R. Thompson, D. Snively, J. Prentice, G. Hodges, and L. Reames, 2012: A Climatology and Comparison of Parameters for Significant Tornado Events in the United States. *Wea. Forecasting*, **27**, 106–123.

Grzych, M., B. Lee, and C. Finley, 2007: Thermodynamic Analysis of Supercell Rear-Flank Downdrafts from Project ANSWERS. *Mon. Wea. Rev.*, **135**, 240–246.

Guarriello, F., C. J. Nowotarski, and C. Epifanio, 2018: Effects of the Low-level Wind Profile on Outflow Position and Near-surface Vertical Vorticity in Supercell Thunderstorms. *J. Atmos. Sci.,* conditionally accepted.

Guo, L., K. Wang, and H. B. Bluestein, 2016: Variability of tornado occurrence over the continental United States since 1950, *J. Geophys. Res. Atmos.*, **121**, 6943–6953.

Ice, R., J. N. Chrisman, J. G. Cunningham, W. D. Zittel, S. D. Smith, O. E. Boydstun, R. D. Cook, and A. K. Heck, 2013: WSR-88D Program Data Quality and Efficiency Enhancements – Plans and Status. Pre-prints, *36th Conf. on Radar Meteorology*, Breckenridge, CO, Amer. Meteor. Soc., 368. [Available online at https://ams.confex.com/ams/36Radar/webprogram/Manuscript/Paper228782/NEXRAD_DQ_Plans_and_Status_Ice_36thRadar_Sept2013_rv2.pdf.]

Kis, A., and J. Straka, 2010: Nocturnal Tornado Climatology. *Wea. Forecasting*, **25**, 545–561.

Klazura, G., and D. Imy, 1993: A Description of the Initial Set of Analysis Products Available from the NEXRAD WSR-88D System. *Bull. Amer. Meteor. Soc.*, **74**, 1293–1311.

Kumjian, M., A. V. Ryzhkov, V. M. Melnikov, and T. J. Schuur, 2010: Rapid-Scan

Super-Resolution Observations of a Cyclic Supercell with a Dual-Polarization WSR-88D. *Mon. Wea. Rev.*, **138**, 3762–3786.

Lakshmanan, V., 2012: *Automating the Analysis of Spatial Grids: A Practical Guide to Data Mining Geospatial Images for Human and Environmental Applications.* Geotech. Env., Vol. 6, Springer, 320 pp.

Lakshmanan, V., A. Fritz, T. Smith, K. Hondl, and G. Stumpf, 2007a: An Automated Technique to Quality Control Radar Reflectivity Data. *J. Appl. Meteor. Climatol.*, **46**, 288–305.

Lakshmanan, V., and T. W. Humphrey, 2014: A MapReduce Technique to Mosaic Continental-Scale Weather Radar Data in Real-Time, *IEEE J. Sel. Topics Appl. Earth Observ. in Remote Sens.*, **7**, 2, 721-732.

Lakshmanan, V., C. Karstens, J. Krause, and L. Tang, 2014: Quality Control of Weather Radar Data Using Polarimetric Variables. *J. Atmos. Oceanic Technol.*, **31**, 1234–1249.

Lakshmanan, V., M. Miller, and T. Smith, 2013: Quality Control of Accumulated Fields by Applying Spatial and Temporal Constraints. *J. Atmos. Oceanic Technol.*, **30**, 745–758.

Lakshmanan, V., T. Smith, K. Hondl, G. Stumpf, and A. Witt, 2006: A Real-Time, Three-Dimensional, Rapidly Updating, Heterogeneous Radar Merger Technique for Reflectivity, Velocity, and Derived Products. *Wea. Forecasting*, **21**, 802–823.

Lakshmanan, V., T. Smith, G. J. Stumpf, and K. Hondl, 2007b: The Warning Decision

Support System – Integrated Information (WDSS-II). *Wea. Forecasting*, **22**, 3, 592-608.

Lakshmanan, V., J. Zhang, and K. Howard, 2010: A Technique to Censor Biological Echoes in Radar Reflectivity Data. *J. Appl. Meteor. Climatol.*, **49**, 453–462.

Lee, R., and A. White, 1998: Improvement of the WSR-88D Mesocyclone Algorithm. *Wea. Forecasting*, **13**, 341–351.

Lemon, L., R. J. Donaldson, D. W. Burgess, and R. A. Brown, 1977: Doppler Radar Application to Severe Thunderstorm Study and Potential Real-Time Warning. *Bull. Amer. Meteor. Soc.*, **58**, 1187–1193.

Lemon, L., and C. Doswell, 1979: Severe Thunderstorm Evolution and Mesocyclone Structure as Related to Tornadogenesis. *Mon. Wea. Rev.*, **107**, 1184–1197.

Lerach, D., and W. Cotton, 2012: Comparing Aerosol and Low-Level Moisture Influences on Supercell Tornadogenesis: Three-Dimensional Idealized Simulations. *J. Atmos. Sci.*, **69**, 969–987.

Maddox, R., J. Zhang, J. Gourley, and K. Howard, 2002: Weather Radar Coverage over the Contiguous United States. *Wea. Forecasting*, **17**, 927–934.

Markowski, P., C. Hannon, J. Frame, E. Lancaster, A. Pietrycha, R. Edwards, and R. Thompson, 2003: Characteristics of vertical wind profiles near supercells obtained from the Rapid Update Cycle. *Wea. Forecasting*, **18**, 1262–1272.

Markowski, P., and Y. Richardson, 2008: The structure and evolution of vortex

lines in supercell thunderstorms. Pre-prints, *24th Conf. on Severe Local Storms*, Savannah, GA, Amer. Meteor. Soc., 4.1. [Available online at https://ams.confex.com/ams/pdfpapers/141560.pdf.]

Markowski, P., and Y. Richardson, 2009: Tornadogenesis: Our Current Understanding, Forecasting Considerations, and Questions to Guide Future Research. *Atmospheric Research*, **93**, 1, 3-10.

Markowski, P., and Y. Richardson, 2010: *Mesoscale Meteorology in Midlatitudes*. Wiley & Sons, Ltd., 407 pp. ISBN 978-0-470-74213-6.

Markowski, P., and Y. Richardson, 2014: The Influence of Environmental Low-Level Shear and Cold Pools on Tornadogenesis: Insights from Idealized Simulations. *J. Atmos. Sci.*, **71**, 243–275.

Markowski, P., Y. Richardson, E. Rasmussen, J. Straka, R. Davies-Jones, and R. Trapp, 2008: Vortex Lines within Low-Level Mesocyclones Obtained from Pseudo-Dual-Doppler Radar Observations. *Mon. Wea. Rev.*, **136**, 3513–3535.

Markowski, P., J. Straka, and E. Rasmussen, 2002: Direct Surface Thermodynamic Observations within the Rear-Flank Downdrafts of Nontornadic and Tornadic Supercells. *Mon. Wea. Rev.*, **130**, 1692–1721.

Miller, M., V. Lakshmanan, and T. Smith, 2013: An Automated Method for Depicting Mesocyclone Paths and Intensities. *Wea. Forecasting*, **28**, 570–585.

Newman, J., V. Lakshmanan, P. Heinselman, M. Richman, and T. Smith, 2013: Range-Correcting Azimuthal Shear in Doppler Radar Data. *Wea. Forecasting*, **28**, 194–211.

Nowotarski, C., and A. Jensen, 2013: Classifying Proximity Soundings with Self-Organizing Maps toward Improving Supercell and Tornado Forecasting. *Wea. Forecasting*, **28**, 783–801.

Nowotarski, C., and P. Markowski, 2016: Modifications to the Near-Storm Environment Induced by Simulated Supercell Thunderstorms. *Mon. Wea. Rev.*, **144**, 273–293.

Potvin, C., K. Elmore, and S. J. Weiss, 2010: Assessing the Impacts of Proximity Sounding Criteria on the Climatology of Significant Tornado Environments. *Wea. Forecasting*, **25**, 3, 921–930.

Radar Operations Center, 2017: NEXRAD AND TDWR Radar Locations. Retrieved from https://www.roc.noaa.gov/WSR88D/Maps.aspx.

Rasmussen, E., and D. Blanchard, 1998: A Baseline Climatology of Sounding-Derived Supercell and Tornado Forecast Parameters. *Wea. Forecasting*, **13**, 1148–1164.

Rinehart, R., 2010: *Radar for Meteorologists*, 5th Ed. Ronald E. Rinehart, 482 pp.

Rotunno, R., and J. Klemp, 1985: On the Rotation and Propagation of Simulated Supercell Thunderstorms. *J. Atmos. Sci.*, **42**, 271–292.

Smith, B., R. L. Thompson, and A. R. Dean, 2014: The Storm Prediction Center Tornadic Storm and Environment Database: Development and Application. Pre-prints, *27th Conf. on Severe Local Storms*, Madison, WI, Amer. Meteor. Soc., 17.1. [Available online at https://ams.confex.com/ams/27SLS/webprogram/Manuscript/Paper254666/SPC_tornadic_storm_environment_database.pdf.]

Smith, B., R. Thompson, J. Grams, C. Broyles, and H. Brooks, 2012: Convective Modes

for Significant Severe Thunderstorms in the Contiguous United States. Part I: Storm Classification and Climatology. *Wea. Forecasting*, **27**, 1114–1135.

Smith, T., and K. L. Elmore, 2004: The Use of Radial Velocity Derivatives to Diagnose Rotation and Divergence. Pre-prints, *22nd Conf. on Severe Local Storms*, Hyannis, MA, Amer. Meteor. Soc., 5.6. [Available online at https://ams.confex.com/ams/pdfpapers/81827.pdf.]

Steiner, M., and J. Smith, 2002: Use of Three-Dimensional Reflectivity Structure for Automated Detection and Removal of Nonprecipitating Echoes in Radar Data. *J. Atmos. Oceanic Technol.*, **19**, 673–686.

Stumpf, G., A. Witt, E. Mitchell, P. Spencer, J. Johnson, M. Eilts, K. Thomas, and D. Burgess, 1998: The National Severe Storms Laboratory Mesocyclone Detection Algorithm for the WSR-88D. *Wea. Forecasting*, **13**, 304–326.

Thompson, R., R. Edwards, J. A. Hart, K. L. Elmore, P. Markowski, 2003: Close Proximity Soundings within Supercell Environments Obtained from the Rapid Update Cycle. *Wea. Forecasting*, **18**, 6, 1243-1261.

Thompson, R., B. Smith, J. Grams, A. Dean, and C. Broyles, 2012: Convective Modes for Significant Severe Thunderstorms in the Contiguous United States. Part II: Supercell and QLCS Tornado Environments. *Wea. Forecasting*, **27**, 1136–1154.

Torres, S., and C. D. Curtis, 2006: Design considerations for improved tornado detection using super-resolution data on the NEXRAD network. Proc. *Fourth European Conf. on Radar in Meteorology and Hydrology*, Barcelona, Spain,

Servei Meteorològic de Catalunya. [Available online at http://cimms.ou.edu/~torres/Documents/ERAD2006.pdf.]

Torres, S., and C. D. Curtis, 2007: Initial implementation of super-resolution data on the NEXRAD network. Pre-prints, *23rd Conf. on Interactive Information Processing Systems (IIPS) for Meteorology, Oceanography, and Hydrology*, San Antonio, TX, Amer. Meteor. Soc., 5B.10. [Available online at https://ams.confex.com/ams/pdfpapers/116240.pdf.]

Trapp, R., G. Stumpf, and K. Manross, 2005: A Reassessment of the Percentage of Tornadic Mesocyclones. *Wea. Forecasting*, **20**, 680–687.

Turner, D., B. M. Lesht, S. A. Clough, J. C. Liljegren, H. E. Revercomb, and D. C. Tobin, 2003: Dry Bias and Variability in Vaisala RS80-H Radiosondes: The ARM Experience. *J. Atmos. Oceanic Technol.*, **20**, 117–132.

University Corporation for Atmospheric Research, 2018: Weather Radar Fundamentals. Retrieved from https://www.meted.ucar.edu/radar/basic_wxradar/print.php.

Weygandt, S., 2017: Rapid Refresh (RAP). Retrieved from https://rapidrefresh.noaa.gov/RRdomains.png.

Whiting, R., and R. Bailey, 1957: Some Meteorological Relationships in the Prediction of Tornadoes. *Mon. Wea. Rev.*, **85**, 141–150.

Wicker, L., 1996: The role of near surface wind shear on low- level mesocyclone generation and tornadoes. Preprints, *18th Conf. on Severe Local Storms*, San Francisco, CA, Amer. Meteor. Soc., 115–119.

Wood, V., and R. Brown, 1997: Effects of Radar Sampling on Single-Doppler Velocity

Signatures of Mesocyclones and Tornadoes. *Wea. Forecasting*, **12**, 928–938.

Wood, V., and R. Brown, 2000: Oscillations in Mesocyclone Signatures with Range Owing to Azimuthal Radar Sampling. *J. Atmos. Oceanic Technol.*, **17**, 90–95.

Wood, V., R. Brown, and D. Sirmans, 2001: Technique for Improving Detection of WSR-88D Mesocyclone Signatures by Increasing Angular Sampling. *Wea. Forecasting*, **16**, 177–184.

Zrnić, D., D. W. Burgess, and L. D. Hennington, 1985: Automatic Detection of Mesocyclonic Shear with Doppler Radar. *J. Atmos. Oceanic Technol.*, **2**, 425–438.

APPENDIX

FIGURES AND TABLES

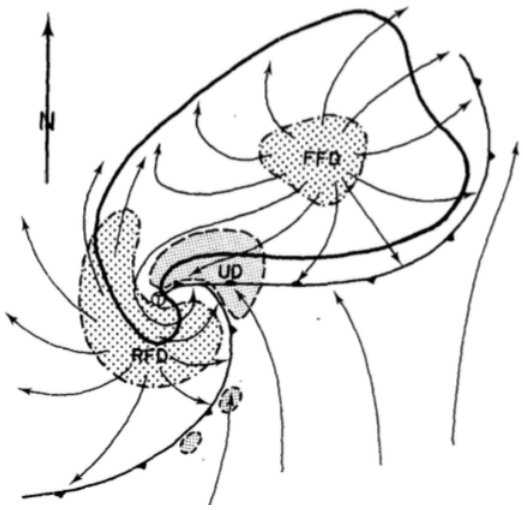

Figure A-1. Diagram of a tornadic supercell. The thick line delineates the radar echo, and conventional frontal symbols mark the gust fronts and occluded wave. Surface locations of the updraft (UD) are finely stippled and both the forward flank downdraft (FFD) and rear flank downdraft (RFD) are coarsely stippled. Streamlines are drawn relative to the ground. The tornado position is indicated by an encircled T. (Reprinted from Lemon and Doswell 1979.)

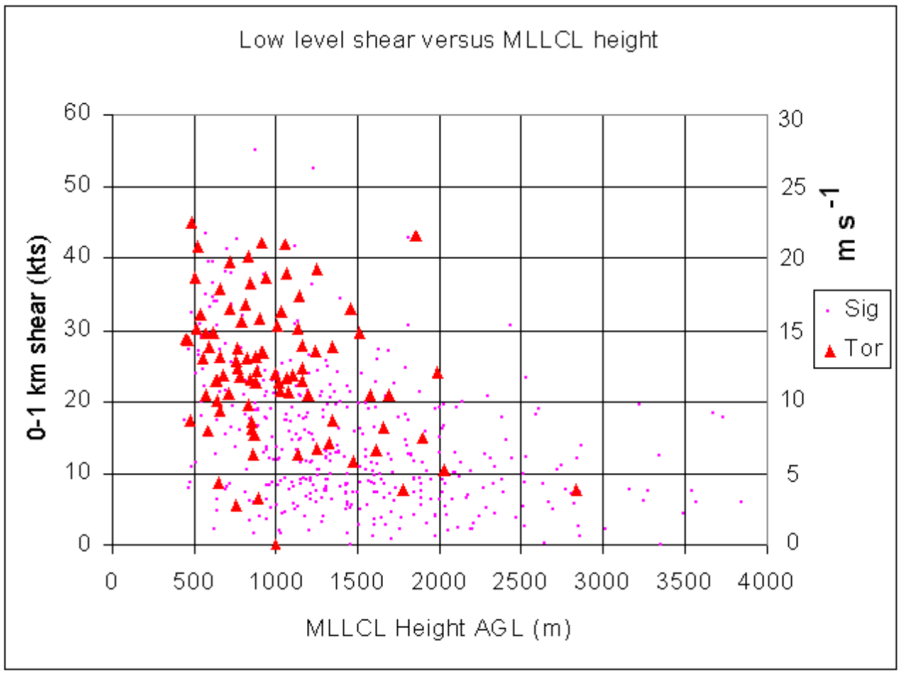

Figure A-2. Plot showing the correlation between LL vertical wind shear and mixed layer LCL (MLLCL) height for both tornadic (triangle) and nontornadic (dot) supercells. This demonstrates that tornadic supercells tend to have lower MLLCL heights and that nontornadic supercells tend to have smaller values of shear. (Reprinted from Craven and Brooks 2002.)

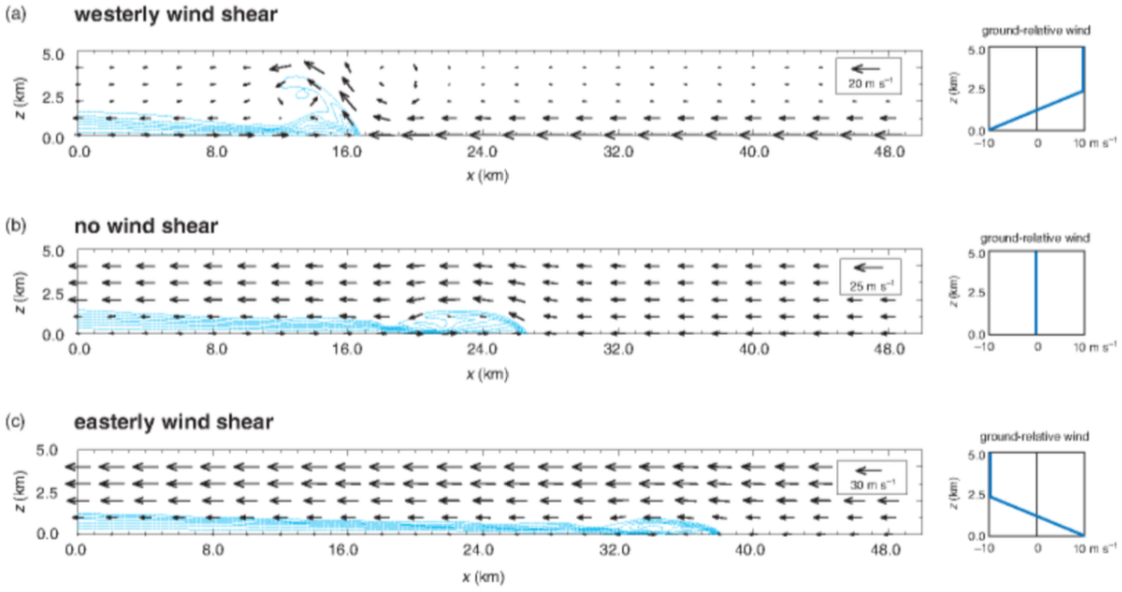

Figure A-3. Numerical simulation of an eastward-moving density current in an environment containing (a) westerly wind shear, (b) no wind shear, and (c) easterly wind shear. Potential temperature perturbations are contoured at 1-K intervals in the cold pool, starting at -1 K. The wind vectors are oriented relative to the density current. The ground-relative wind profiles are shown on the right. (Reprinted from Markowski and Richardson 2010.)

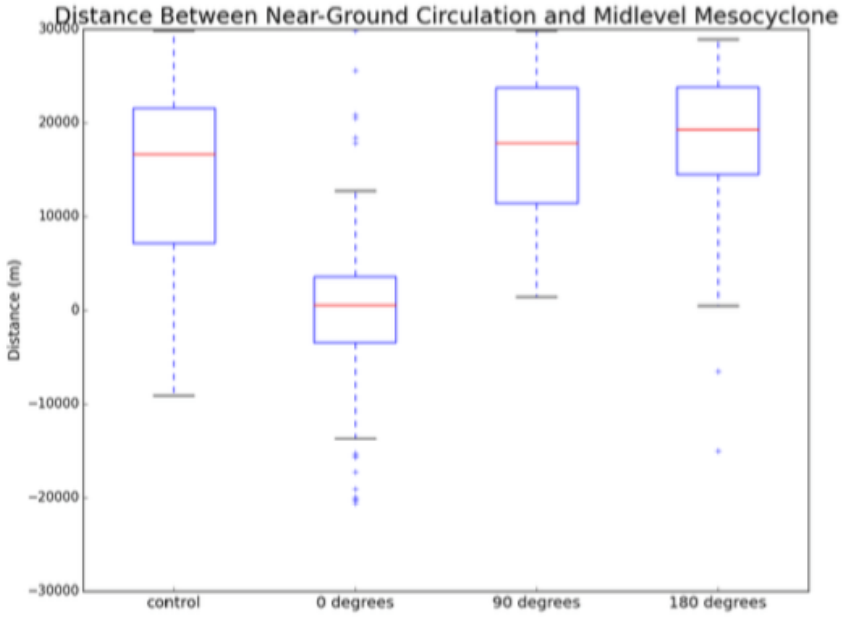

Figure A-4. Box plots showing an orientation of LL vertical wind shear that produced the smallest mean mesocyclone tilt in simulated supercells. A 0-degree orientation refers to easterly shear, and a 180-degree orientation refers to westerly shear. (Reprinted from Guarriello et al. 2018.)

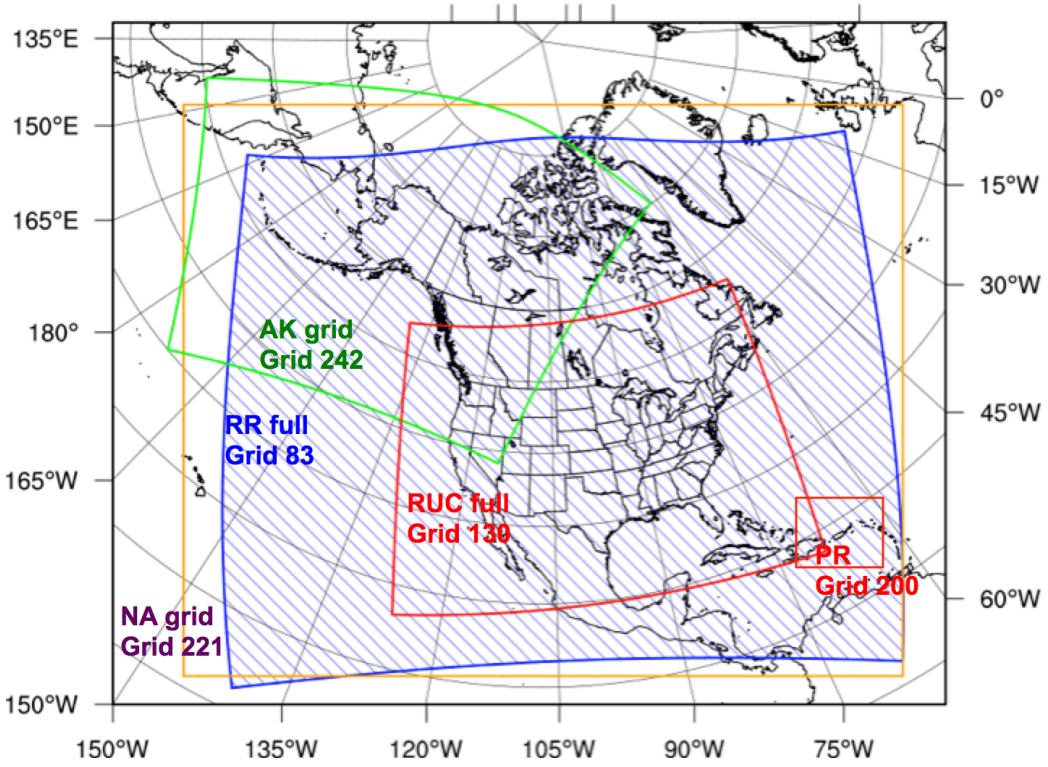

Figure A-5. Map of RUC-2 (red) and RAP (blue) model domains. Note that the RUC-2 only encompasses the CONUS. (Reprinted from Weygandt 2017, https://rapidrefresh.noaa.gov/RRdomains.png.)

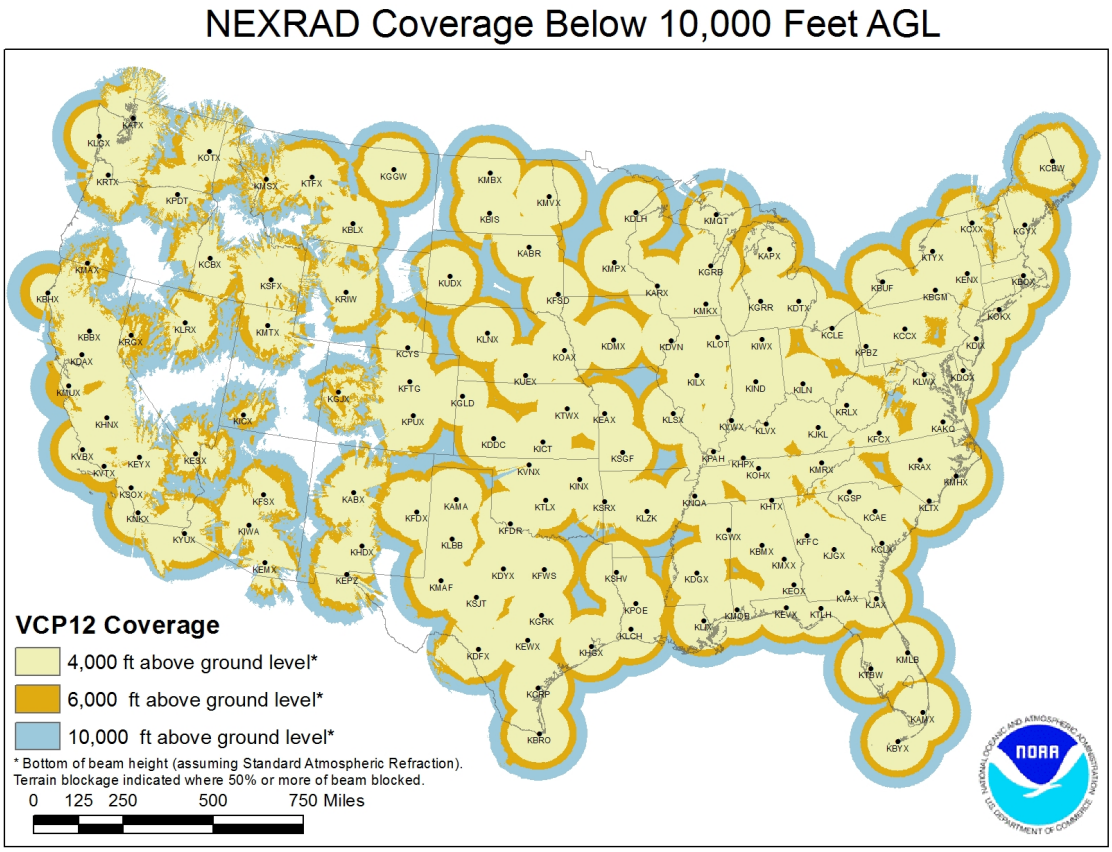

Figure A-6: Spatial coverage of the WSR-88D radar network across the CONUS. (Reprinted from Radar Operations Center 2017, https://www.roc.noaa.gov/WSR88D/Maps.aspx.)

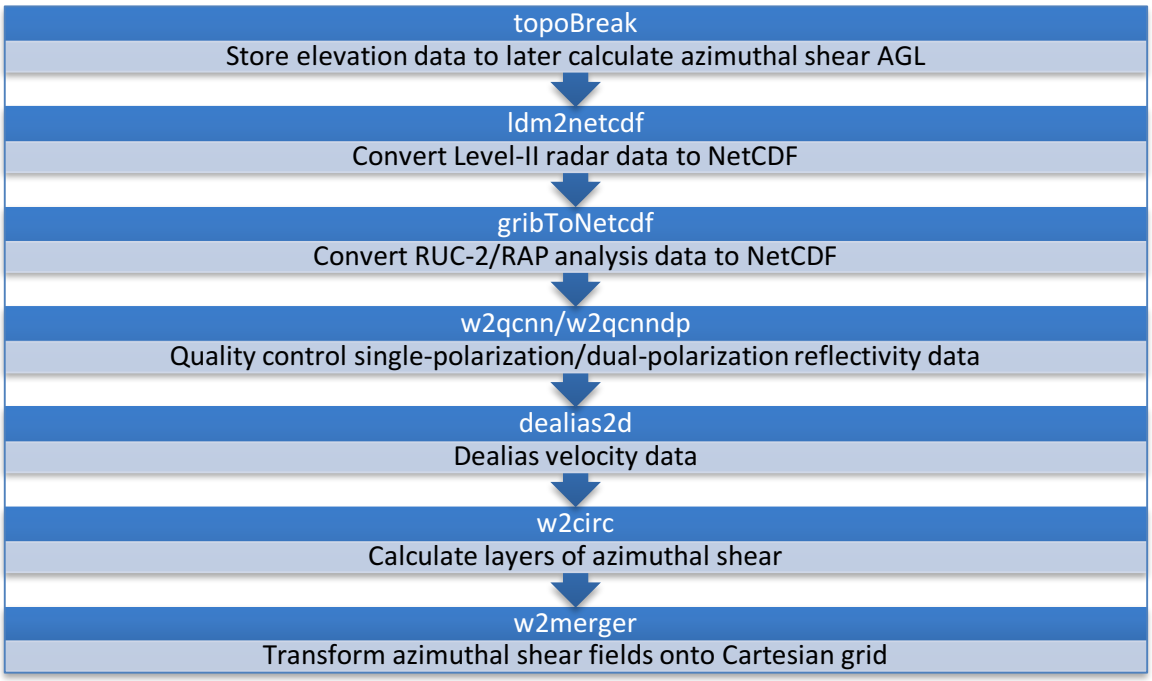

Table A-1. Flowchart of the progression of the WDSS-II algorithms used to process data, calculate azimuthal shear, and transform onto Cartesian grid (Lakshmanan et al. 2007b).

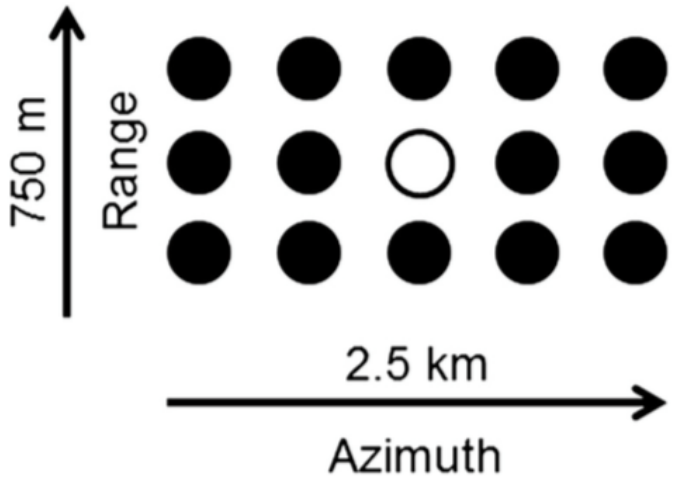

Figure A-7. Schematic of the concept for LLSD shear calculation. Black circles represent radar-sampling volumes in azimuth and range, and the shear of the center (white) circle is calculated with velocity data from the surrounding (black) circles. (Reprinted from Newman et al. 2013.)

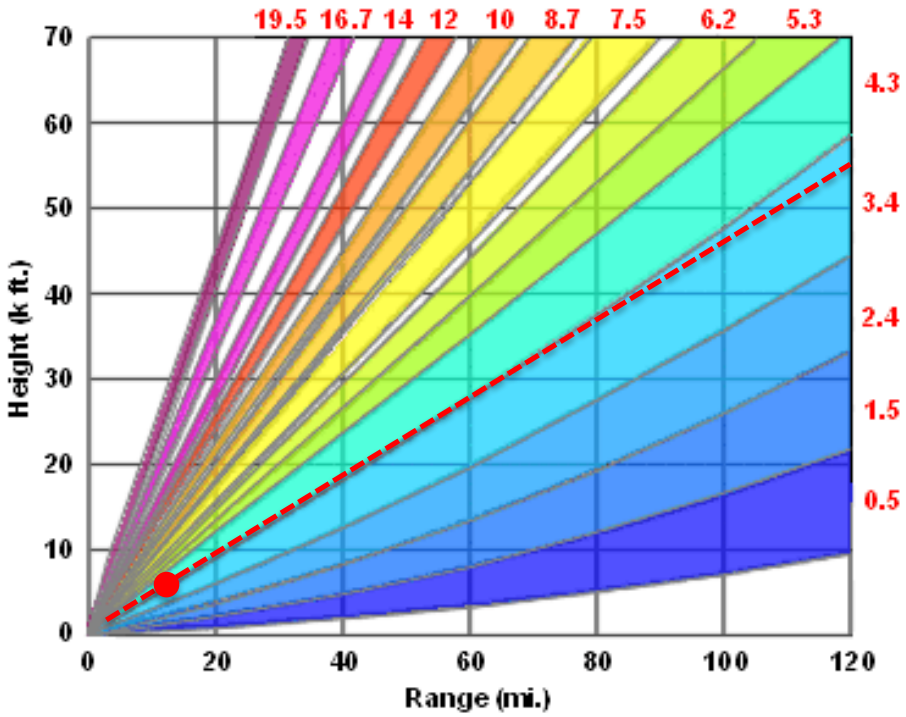

Figure A-8. Schematic illustrating the correction done to account for radar scan time lapse. In this example, the red circle indicates the ML mesocyclone of a supercell, and the red dashed line marks the elevation scan that measured the ML mesocyclone, which depends on range. Using that information, the following equation was used to calculate a distance correction: (fraction of elevation scan to total elevation scans * average volume scan duration) * storm motion = distance correction. An average volume scan duration length of 4.5 minutes was used, which is appropriate for severe weather volume coverage patterns. (Adapted from University Corporation for Atmospheric Research 2018, https://www.meted.ucar.edu/radar/basic_wxradar/print.php).

a)

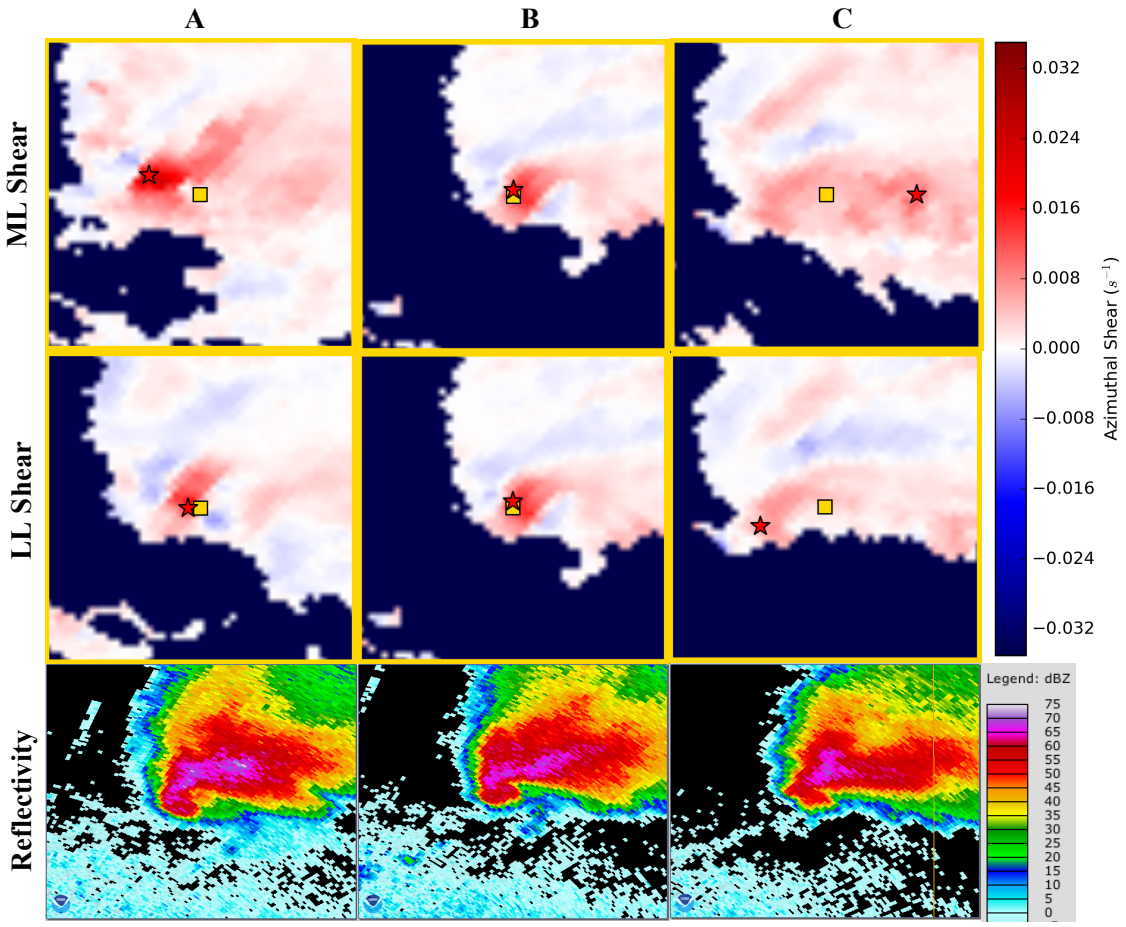

Figure A-9. a) Panels showing the progression of the 05 June 2009 tornadic supercell in Wyoming. The panels include rows of ML azimuthal shear and LL azimuthal shear, centered on the corresponding MDA (gold square), and marking the location of maximum shear (red star). The rows of LL reflectivity coincide with the same portions of the supercell and are also centered on the MDA. The lettered columns refer to the letters on the time series. The time series (b) shows the evolution of the corrected mesocyclone tilt (solid black), observed mesocyclone tilt (dashed gray), and smoothed mesocyclone tilt (solid blue) during the lifetime of the storm. The smoothed line was created using a 3-point moving average of the corrected tilt values. The x-axis depicts the minutes before (negative) and after (positive) the beginning of the tornado, the duration of which is indicated by gray shading. A skew-T (c) and hodograph (d) depicting the inflow environment are also shown. The LCL and CAPE values shown on the skew-T are different from the calculated values and should be disregarded.

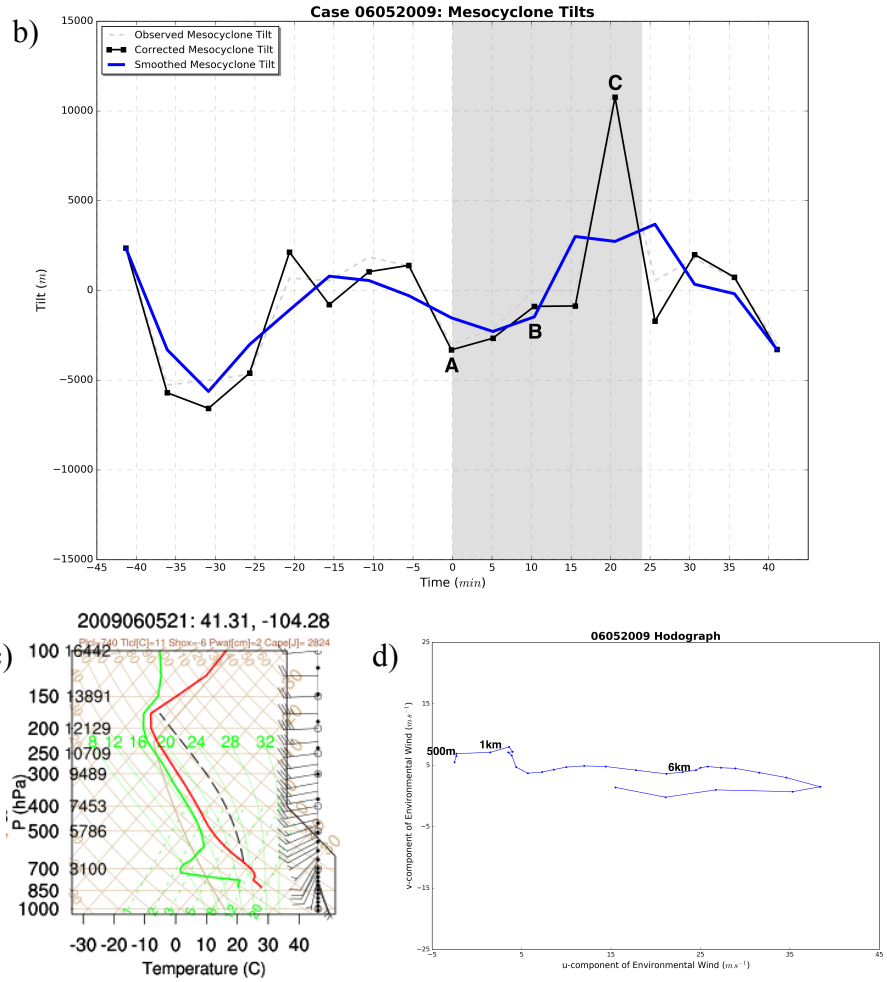

Figure A-9. Continued.

a)

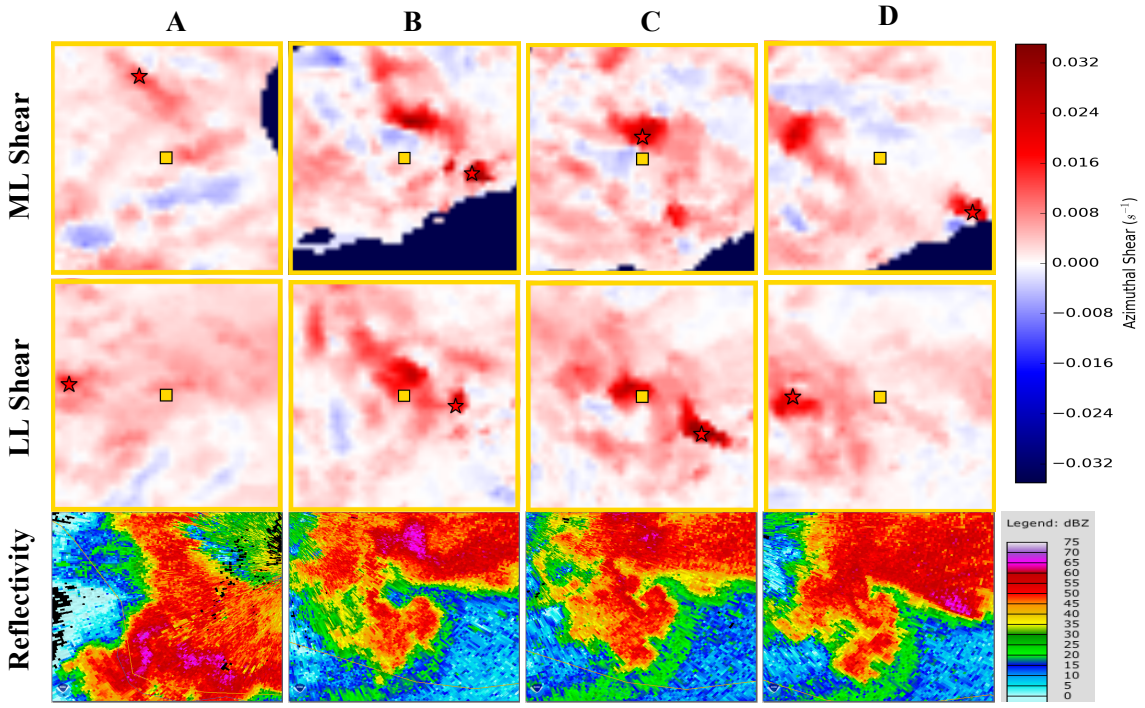

Figure A-10. As in Figure A- 9, except for the 18 April 2013 tornadic supercell. The ML azimuthal shear at time A (panel a) shows that the supercell was in the vicinity of the radar cone of silence, but this did not affect MDA identification of the mesocyclone.

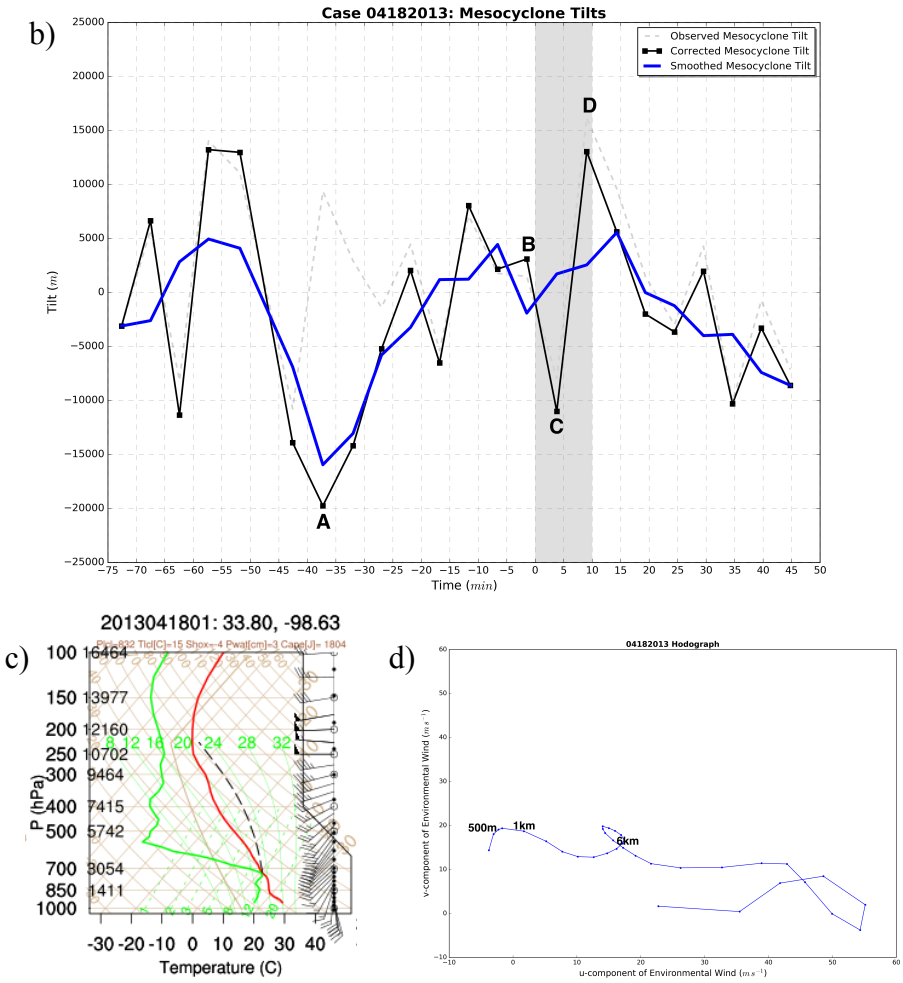

Figure A-10. Continued.

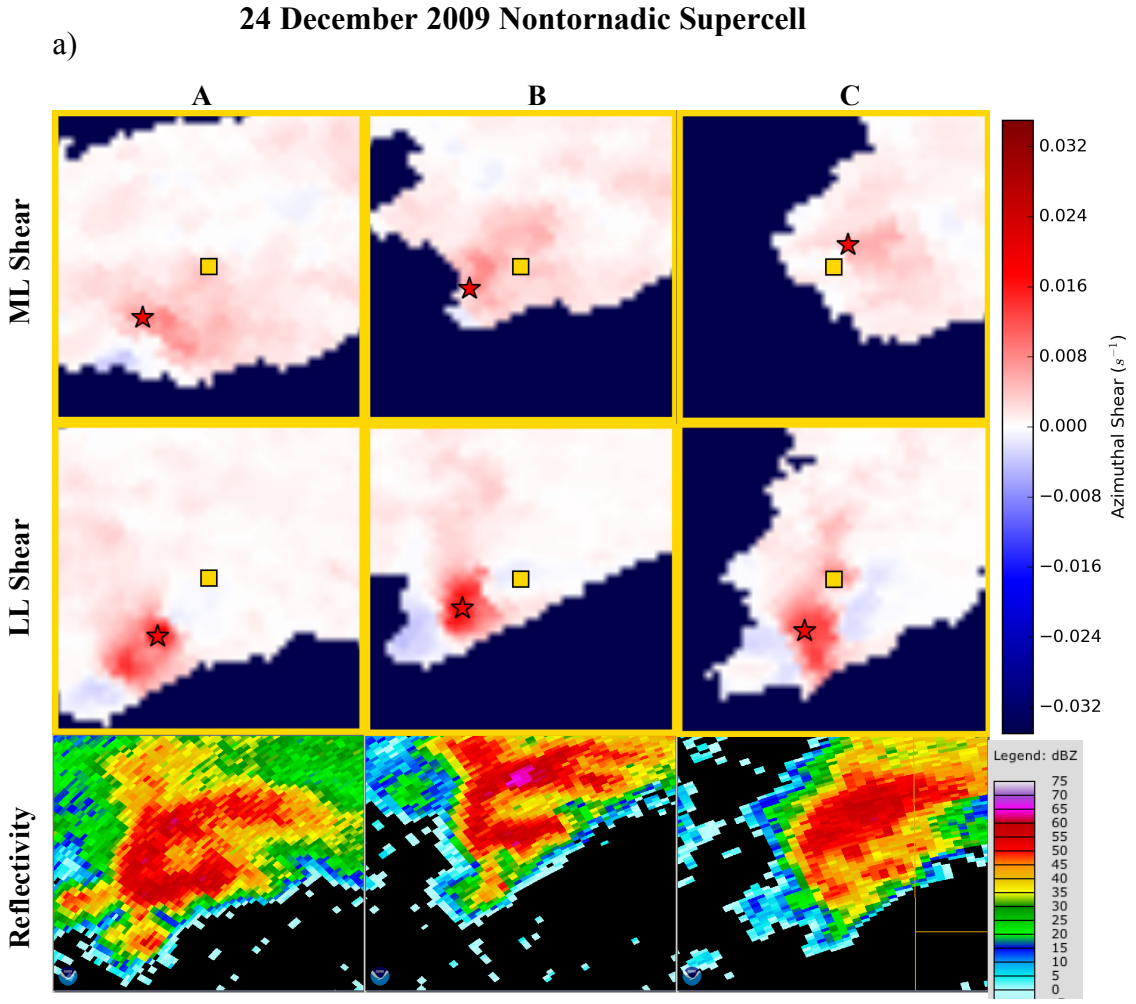

Figure A-11. As in Figure A- 9, except for the 24 December 2009 nontornadic supercell. In the time series (b), the zero on the time axis represents the midpoint of the supercell.

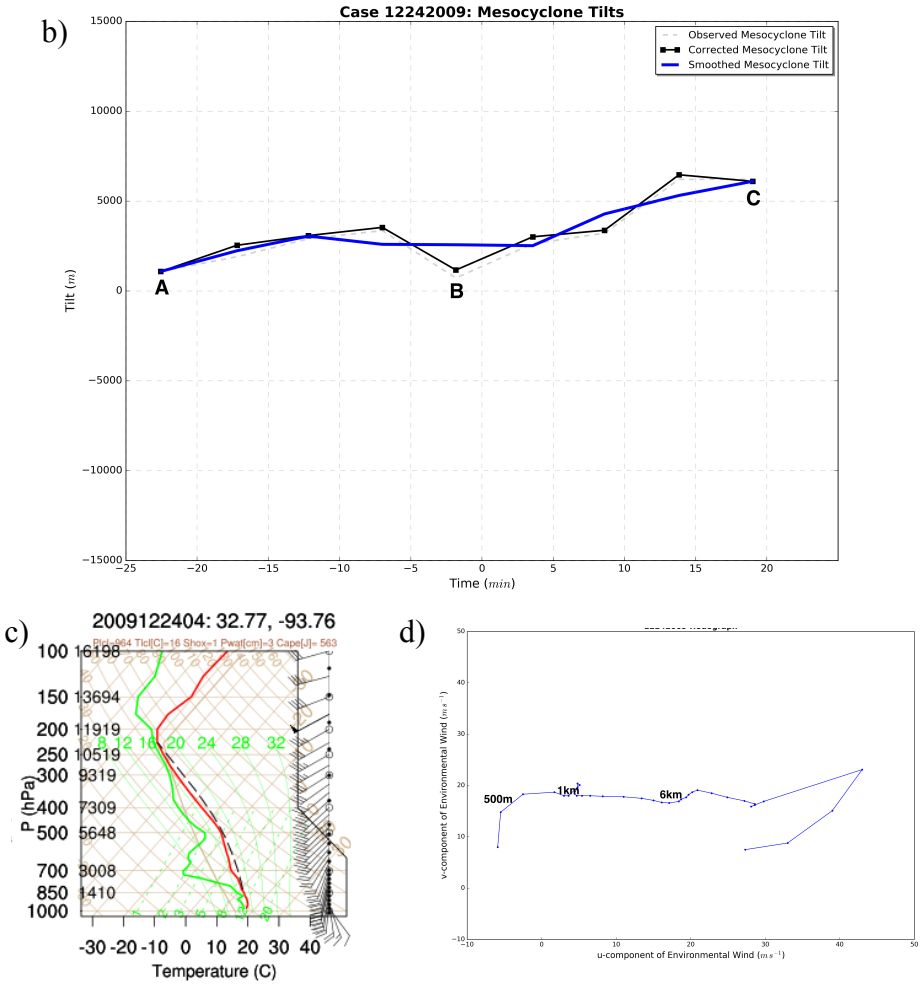

Figure A-11. Continued.

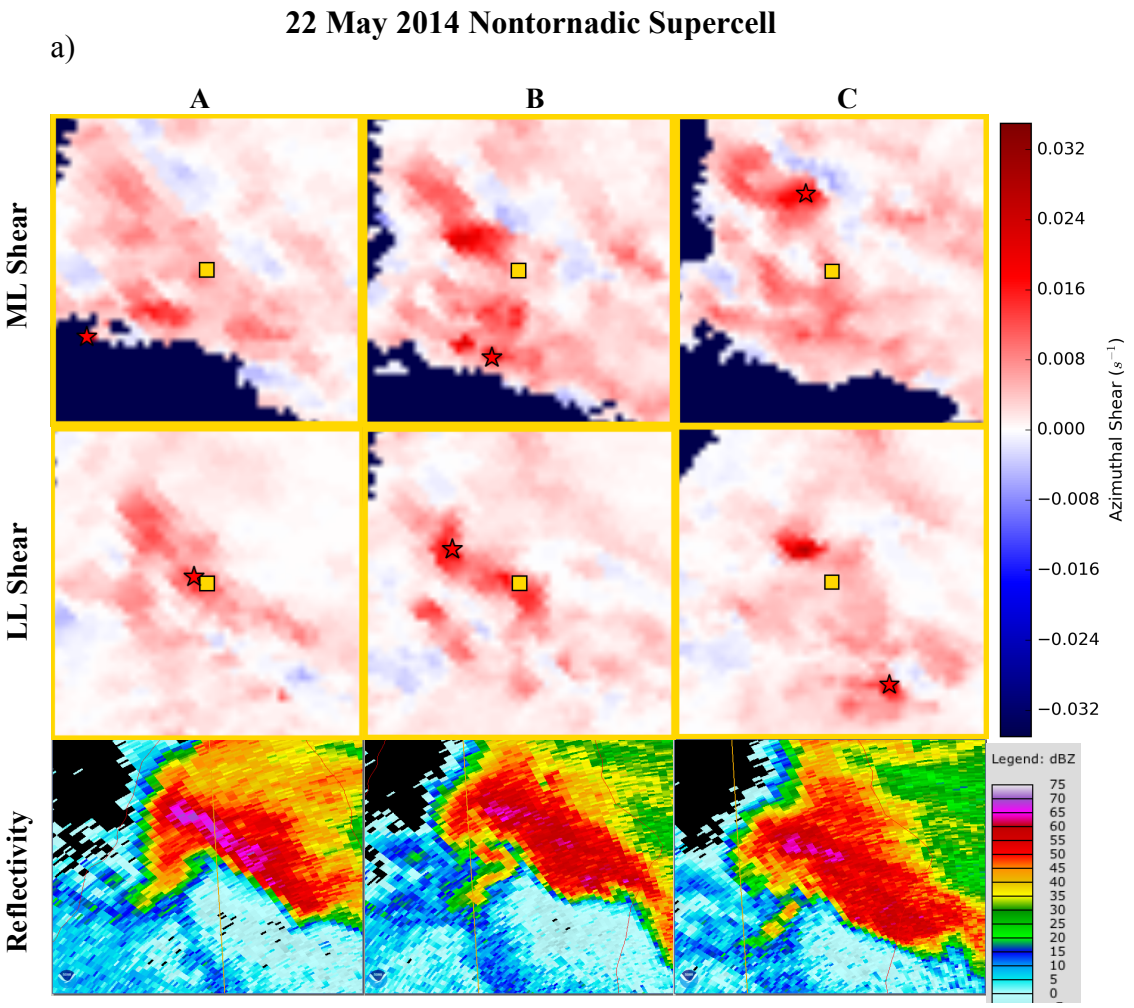

Figure A-12. As in Figure A- 11, except for the 22 May 2014 nontornadic supercell.

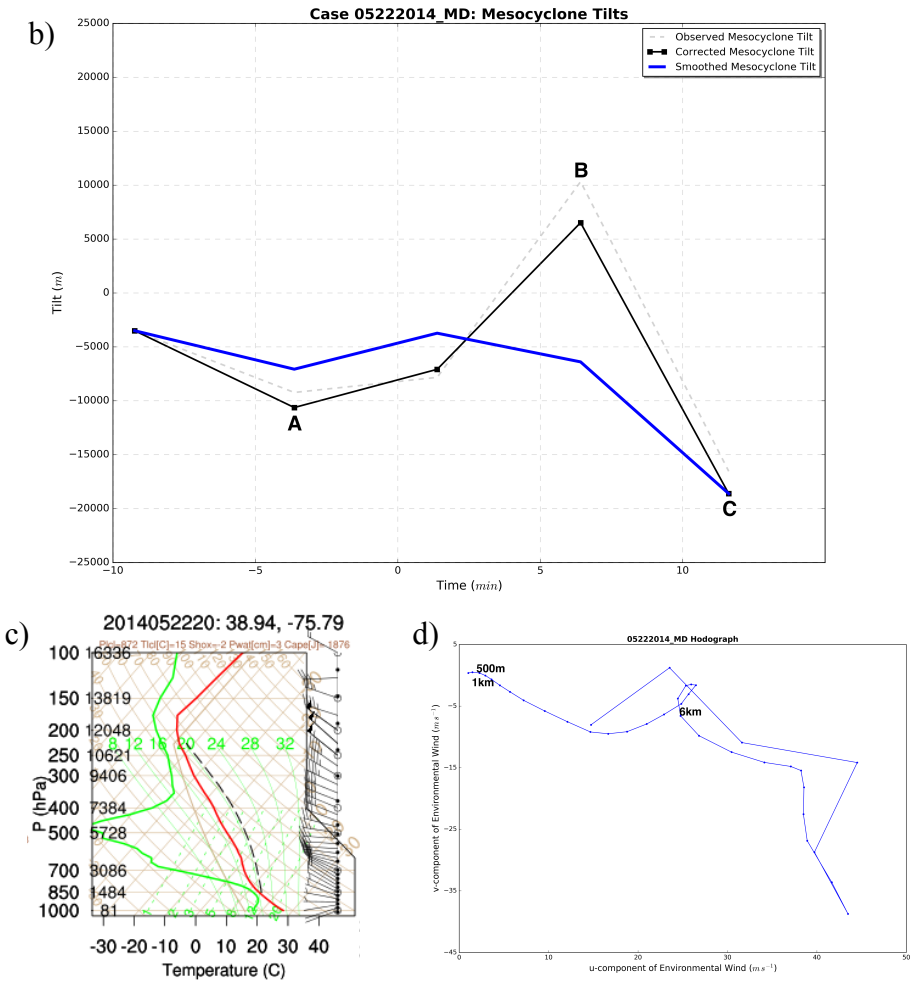

Figure A-12. Continued.

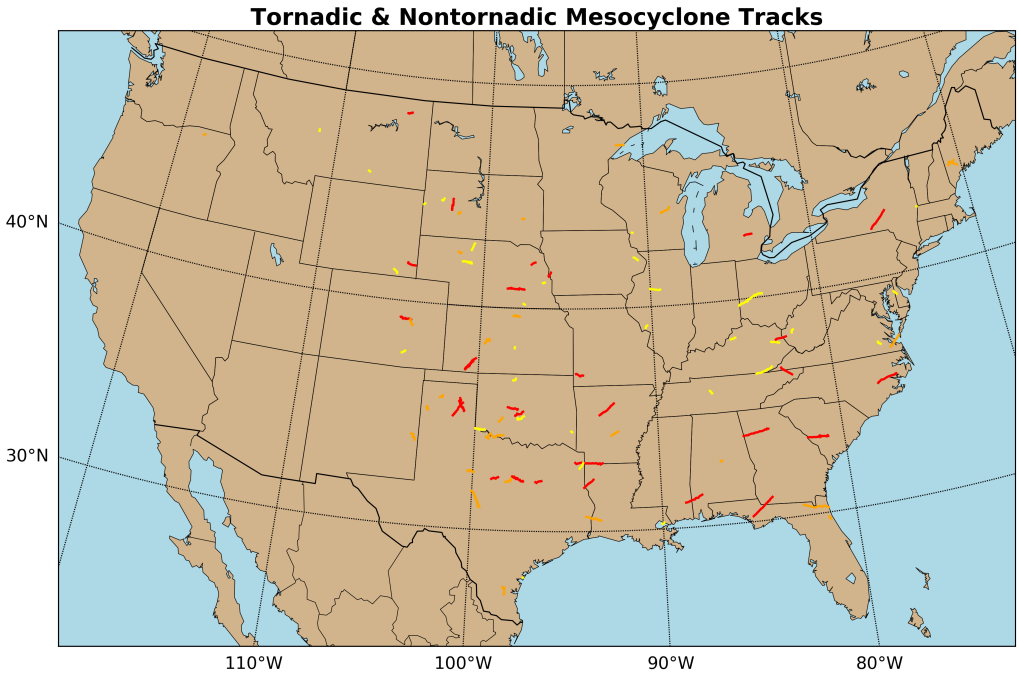

Figure A-13. Map of the CONUS depicting 88 mesocyclone tracks, as defined by the MDA. There are 32 nontornadic (yellow) mesocyclones, 27 weakly tornadic (orange), and 29 significantly tornadic (red). Fifty-three of them occurred in the spring, 24 in the summer, 8 in the fall, and 3 in the winter.

a)

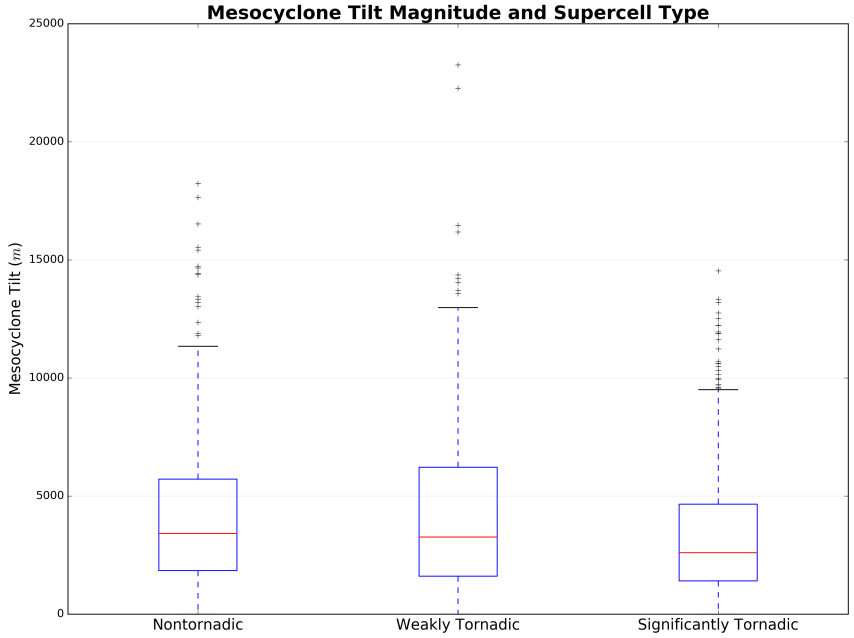

b)

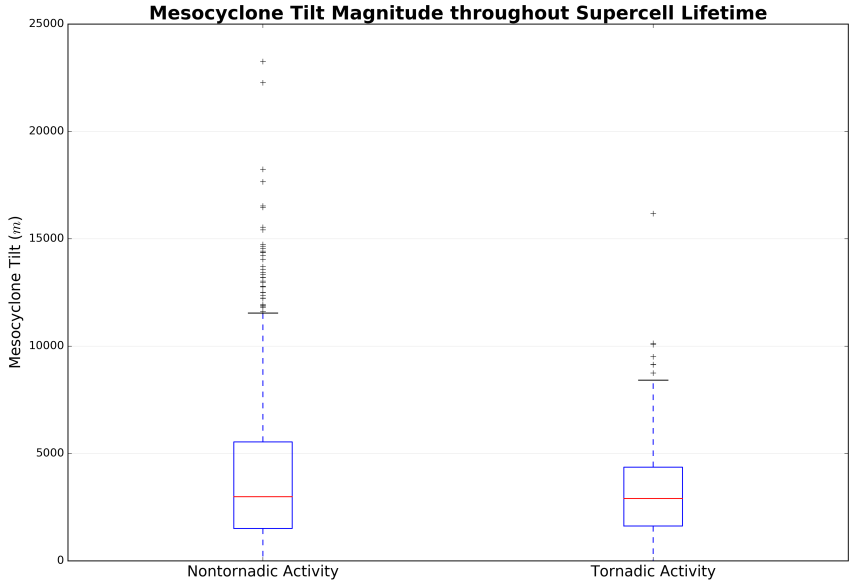

Figure A-14. a) Boxplots showing the mesocyclone tilt for each supercell type, at every radar scan. The tilt throughout the duration of each supercell is represented. b) Boxplots showing the mesocyclone tilt at every radar scan, during periods of nontornadic and tornadic activity. The median (red bar), lower and upper quartiles (Q1 and Q3, blue bars), data range (Q1-1.5IQR and Q3+1.5IQR, black bars), and outliers (black crosses) are displayed.

a)

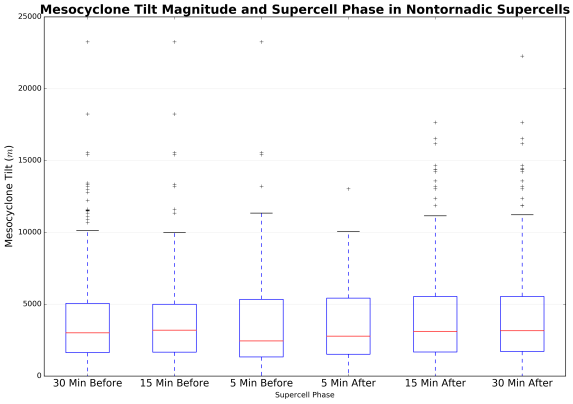

b)

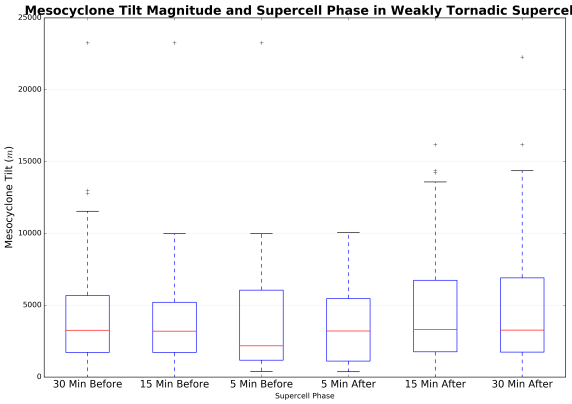

c)

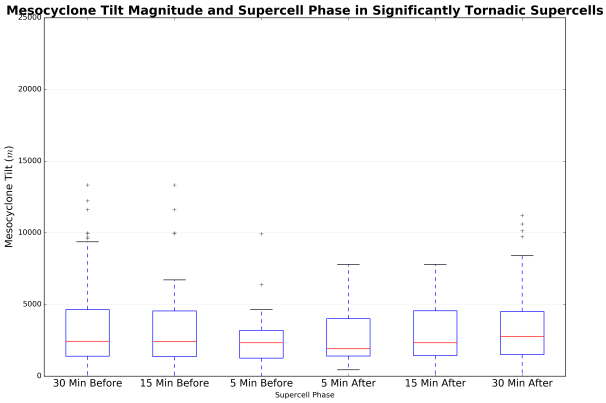

Figure A-15. Boxplots showing the evolution of the mesocyclone tilt in the minutes before and after the middle of nontornadic supercells (a) and before and after the beginning of tornadoes in weakly tornadic (b) and significantly tornadic (c) supercells.

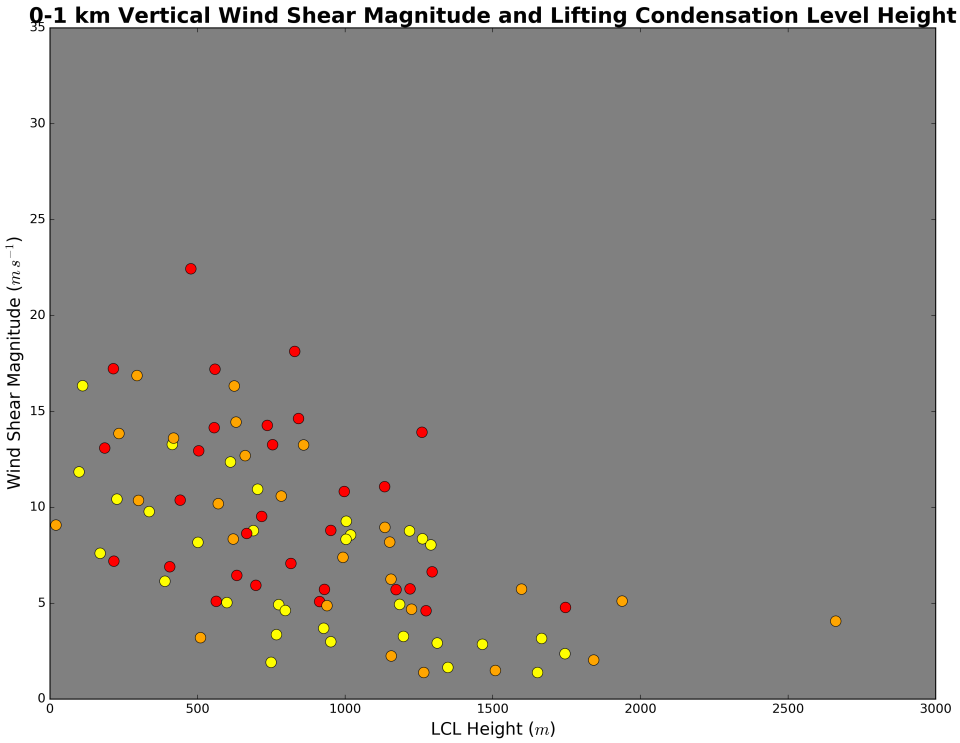

Figure A-16. Reproduction of Figure 12 in Craven and Brooks (2002; herein, Figure A-2). The values of 0-1 km vertical wind shear and LCL height are shown for nontornadic (yellow), weakly tornadic (orange), and significantly tornadic (red) supercells.

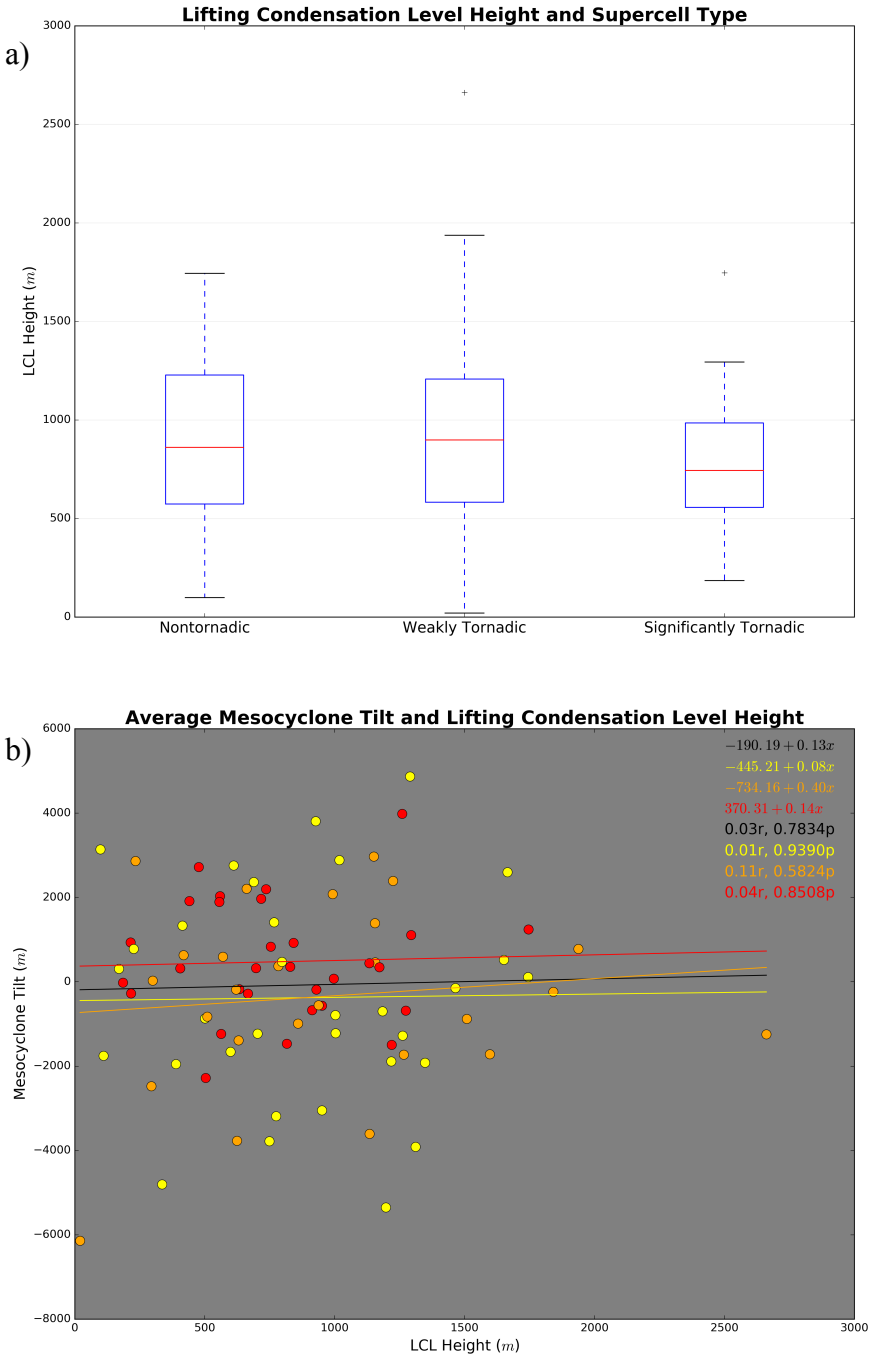

Figure A-17. a) Boxplots showing LCL height for every type of supercell. b) Plot showing correlation between LCL height and average mesocyclone tilt for each type of supercell. Least squares linear regression lines are colored according to supercell type, with their equations displayed. Pearson correlation coefficients, with their associated p-values, are displayed and colored according to supercell type. A confidence level of 95% (α=0.05) was used.

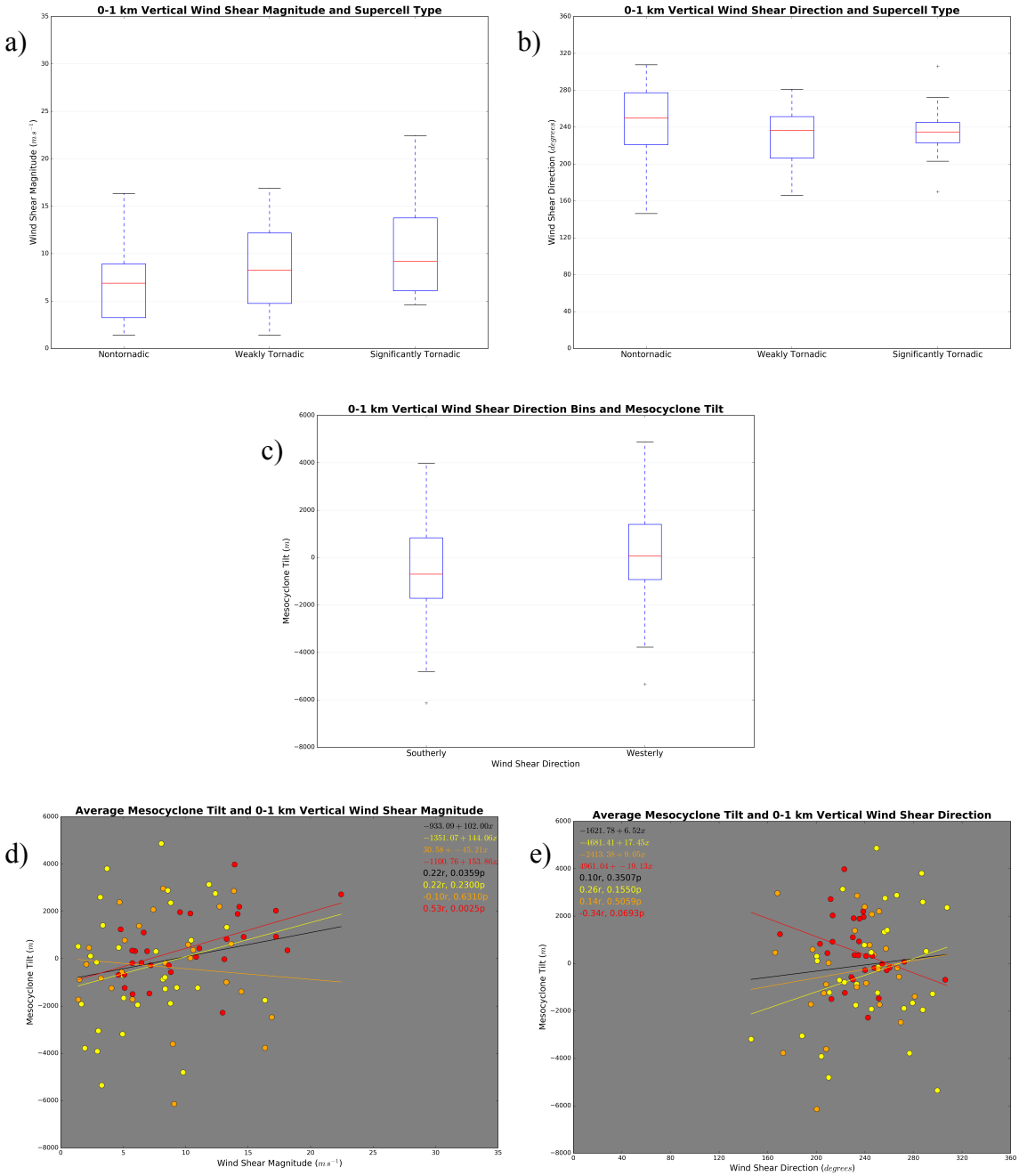

Figure A-18. Boxplots showing 0-1 km vertical wind shear magnitude (a) and direction (b) for every type of supercell. c) Boxplots showing 0-1 km vertical wind shear directions binned into southerly and westerly. None of the cases had shear from the north or the east. Plots showing the correlation between average mesocyclone tilt and 0-1 km vertical wind shear magnitude (d) and direction (e).

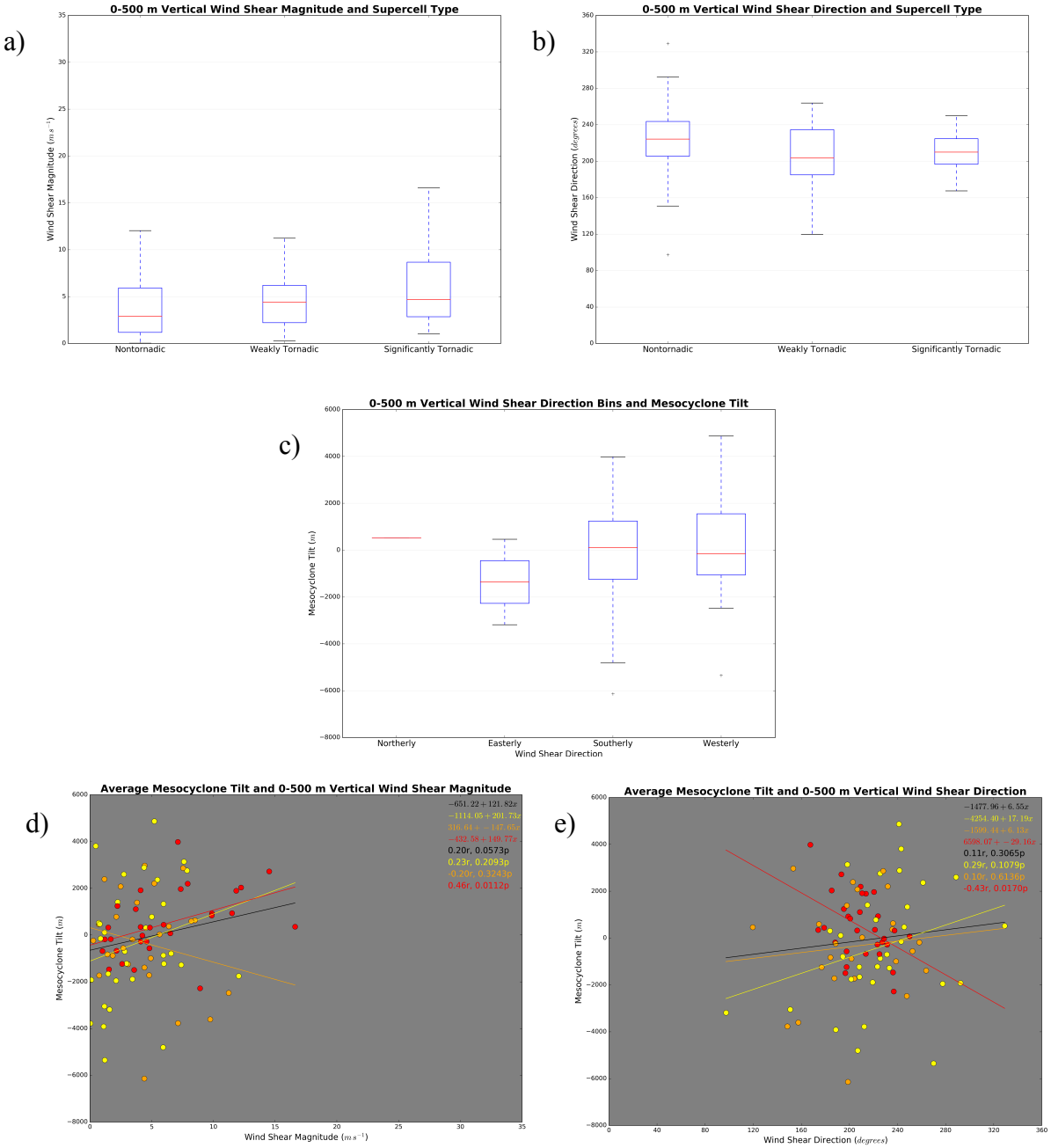

Figure A-19. Boxplots showing 0-500 m vertical wind shear magnitude (a) and direction (b) for every type of supercell. c) Boxplots showing 0-500 m vertical wind shear directions binned into northerly (1 case), easterly (2 cases), southerly, and westerly. Plots showing the correlation between average mesocyclone tilt and 0-500 m vertical wind shear magnitude (d) and direction (e).

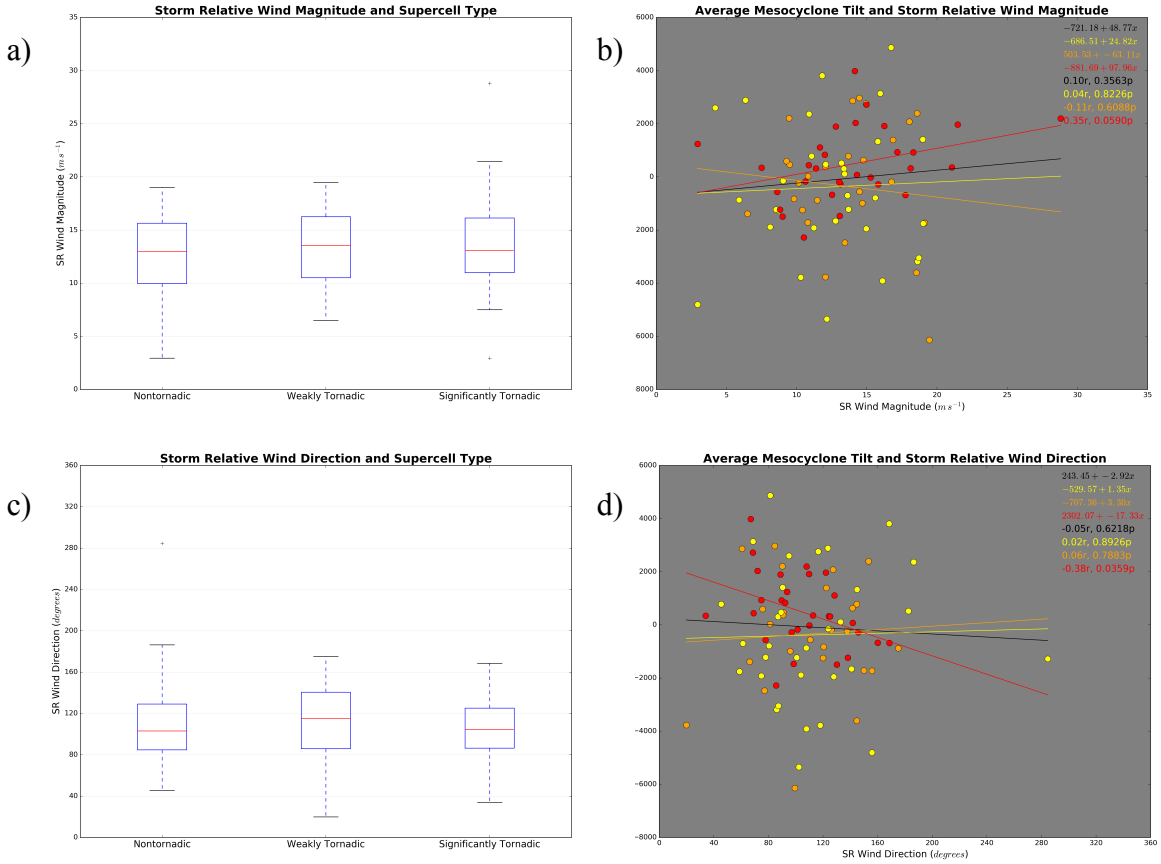

Figure A-20. a) Boxplots showing the surface SR wind magnitude for every supercell type. b) Plot showing correlation between average mesocyclone tilt and surface SR wind magnitude. c) Boxplots showing the surface SR wind direction for every supercell type. d) Plot showing correlation between average mesocyclone tilt and surface SR wind direction.

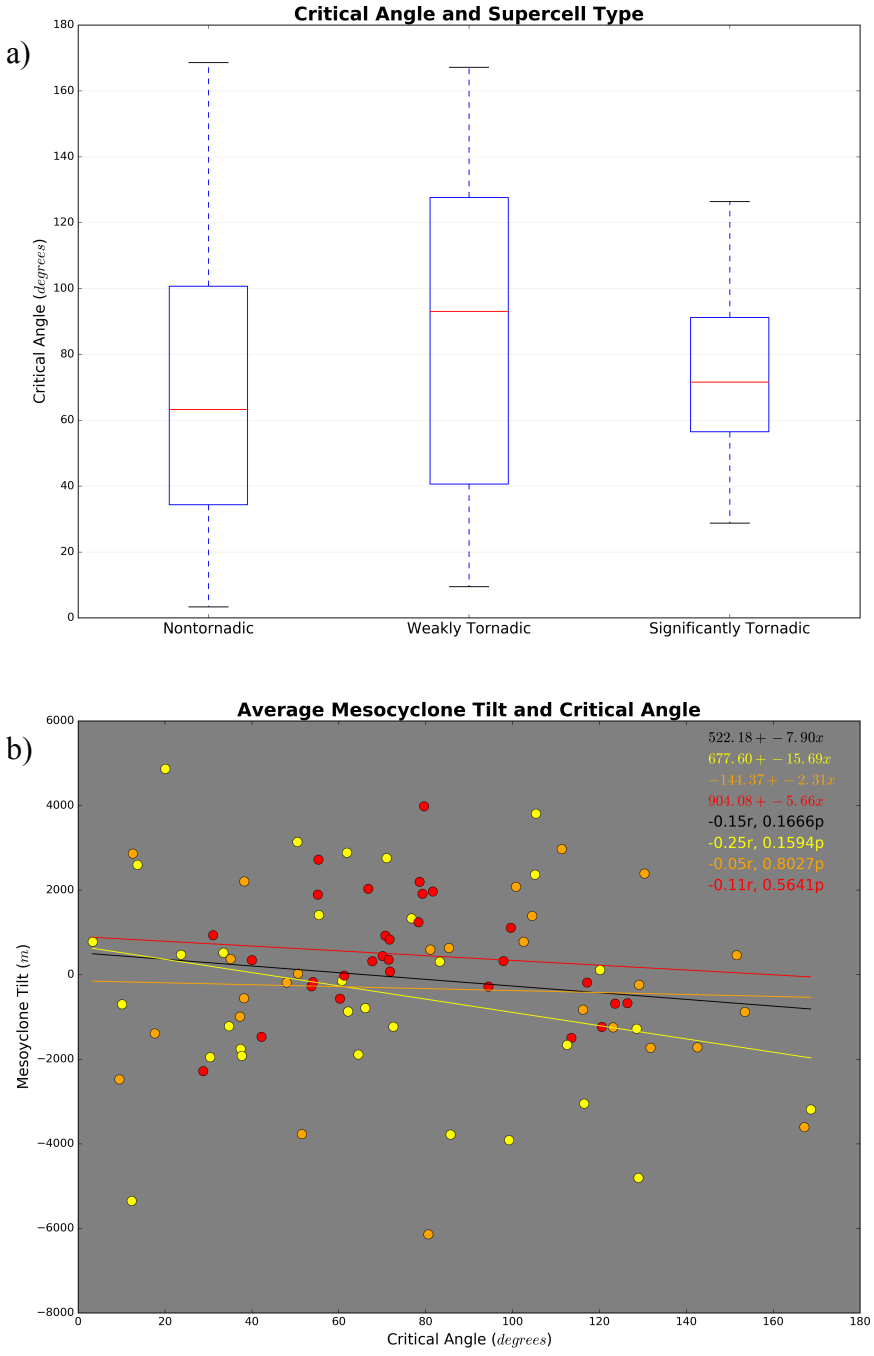

Figure A-21. a) Boxplots showing critical angle values for every supercell type. b) Plot showing correlation between average mesocyclone tilt and critical angle.